Clemson University
TigerPrints

All Theses Theses

December 2020

Effect of Carbon Black Electrocatalyst Thickness and Composition on Electrosynthesis of Hydrogen Peroxide on Gas Diffusion Electrodes

Lauren Marie Schmidt
Clemson University, lms529@bellsouth.net

Follow this and additional works at: https://tigerprints.clemson.edu/all_theses

Recommended Citation
Schmidt, Lauren Marie, "Effect of Carbon Black Electrocatalyst Thickness and Composition on Electrosynthesis of Hydrogen Peroxide on Gas Diffusion Electrodes" (2020). *All Theses*. 3465.
https://tigerprints.clemson.edu/all_theses/3465

This Thesis is brought to you for free and open access by the Theses at TigerPrints. It has been accepted for inclusion in All Theses by an authorized administrator of TigerPrints. For more information, please contact kokeefe@clemson.edu.

EFFECT OF CARBON BLACK ELECTROCATALYST THICKNESS AND COMPOSITION ON ELECTROSYNTHESIS OF HYDROGEN PEROXIDE ON GAS DIFFUSION ELECTRODES

A Thesis
Presented to
the Graduate School of
Clemson University

In Partial Fulfillment
of the Requirements for the Degree
Master of Science
Environmental Engineering and Science

---

by
Lauren Marie Schmidt
December 2020

Accepted by
Dr. Sudeep Popat, Committee Chair
Dr. Elizabeth Carraway
Dr. David Ladner

ABSTRACT

The in-situ electrosynthesis of hydrogen peroxide (H_2O_2) from reduction of oxygen is a promising method to produce a strong oxidant and disinfectant for application in the water and wastewater treatment industry. Capable of producing low concentrations of H_2O_2 with no aeration requirements and harmless by-products of water and oxygen, the electrosynthesis of H_2O_2 using gas diffusion electrodes is advantageous. This research examines the impact that electrocatalyst thickness and composition have on the production efficiency of H_2O_2 at the gas diffusion layer of a gas diffusion electrode. From these results, the optimum electrocatalyst loading and composition with its respective energy requirements is assessed.

An increase in electrocatalyst loading on the gas diffusion layer saw a greater thickness of the electrocatalyst layer, increasing the perpendicular diffusion pathway required for H_2O_2 to reach the electrolyte solution. At a current density of 1 mA/cm^2, the lowest electrocatalyst loading of 0.5 mg/cm^2 produced the highest H_2O_2 concentration of 807.54 mg/L and maximum current coulombic efficiency of 53%. The H_2O_2 produced from the additional three electrocatalyst loadings of 1.5, 3.0, and 5.0 mg/cm^2 decreased linearly with increasing loading. An increase in the length of the diffusion pathway allows more time for H_2O_2 to accumulate and degrade to H_2O or O_2. As current density was increased, higher yields of H_2O_2 were achieved for all loadings, suggesting less chemical degradation of H_2O_2 to O_2 as the higher electrocatalyst loadings significantly improved current efficiencies to match the lower electrocatalyst loadings. An energy input analysis calculating the mass produced/energy input in kg H_2O_2/kWh demonstrated

a benefit in selecting higher electrocatalyst loadings at higher current densities. Although the highest electrocatalyst loading of 5.0 mg/cm^2 produced the lowest concentrations of H_2O_2 at a current density of 5 mA/cm^2, it accomplishes the greatest mass produced/energy input of 3.84 kg H_2O_2/kWh.

The effect of electrocatalyst composition was examined as electrocatalyst loadings of 1.5 and 5.0 mg/cm^2 were tested with and without proton exchange polymer, Nafion, in the electrocatalyst carbon ink. The electrocatalyst loadings comprised of a carbon ink without Nafion resulted in greater H_2O_2 concentrations and current efficiencies, with smaller differences between loadings compared to the results for loadings containing Nafion. At the cathode surface, pH increases rapidly, where H_2O_2 exists as its anion, hydroperoxide (HO_2^-). Interaction with the negatively charged sulfonic groups (SO_3^-) in the proton exchange polymer, Nafion, causes resistance to the mass transport of HO_2^- through the electrocatalyst layer. The HO_2^- can then accumulate, be degraded, and result in lower measured concentrations of H_2O_2 in the electrolyte.

ACKNOWLEDGEMENTS

I want to express my utmost gratitude to my advisor, Dr. Sudeep Popat, for the opportunity to conduct this research and work alongside his talented research group. He supported me throughout the last year and a half with valuable guidance, even through a late research topic change, to ensure I would achieve my goals. My committee members, Dr. David Ladner and Dr. Elizabeth Carraway, have been incredibly supportive and encouraging throughout my time at Clemson. They are more than gifted professors, but also mentors with passion for their work, inspiring me to achieve greatness in this field.

I also want to thank Spencer Lindsay for his advice and assistance with experiments. From the start, he set me up for success with his patience and training. Additionally, I would like to acknowledge George Wetzel for his help with SEM, Dr. Apparao Rao and Nawraj Sapkota for their work on Raman, and Rodney Merck and Rodney Morgan for machining the materials for the electrochemical cell reactors.

Finally, I thank God for blessing me with this gift of a life. He has gifted with my family, whom I owe sincerest thanks for their unconditional love and care every day. I am incredibly fortunate to have two parents and a brother who motivate me to pursue my dreams and provide unlimited support to ensure I get to live my best life.

TABLE OF CONTENTS

Page

ABSTRACT ii
ACKNOWLEDGEMENTS iv
LIST OF TABLES vii
LIST OF FIGURES viii
LIST OF SYMBOLS AND ABBREVIATIONS xi
1.0 INTRODUCTION 1
2.0 BACKGROUND 3
2.1 Industrial Production and Applications 3
2.2 Microbial Fuel Cells 5
2.3 Microbial Peroxide Producing Cells 6
2.4 Gas Diffusion Electrodes 8
2.5 Electrocatalysts 10
2.6 Cathode Design 11
3.0 RESEARCH OBJECTIVES 13
4.0 MATERIALS AND METHODS 15
4.1 Electrochemical Cell 15
4.2 Electrocatalyst Preparation 17
4.3 Cathode Preparation 18
4.4 Electrochemical Techniques 19
4.5 H_2O_2 Production Experiments 19
4.6 H_2O_2 Measurement 20
4.7 SEM Imaging 22
5.0 RESULTS AND DISCUSSION 23
5.1 Effect of Electrocatalyst Loading on H_2O_2 Production 23
5.1.1 Effect of Current Density 26
5.1.2 Energy Input Analysis 34
5.2 Effect of Electrocatalyst Loading on Cathode Structure 36
5.2.1 SEM Images 36

Table of Contents (continued)

Page

5.3 Effect of Electrocatalyst Ink Composition on H_2O_2 Production 40
5.3.1 SEM Images 43
5.4 Other Considerations 44
6.0 CONCLUSION 47
6.1 Assessment of Research Objectives 47
7.0 FUTURE WORK 50
APPENDICES 52
Appendix A – Pictures of electrochemical cell reactor and materials.....53
Appendix B – Vulcan XC 72 properties.....55
Appendix C – pH data 56
Appendix D – Additional SEM images for electrocatalyst loading experiments.....58
REFERENCES 59

LIST OF TABLES

Page

Table 1. Energy input comparison of H_2O_2 production at two current densities.....35

Table B-1. Physical and chemical properties of Vulcan XC 72 carbon powder. 55

LIST OF FIGURES

Page

Figure 1. Schematic of MPPC which reduces oxygen to H_2O_2 at the cathode with bacteria to oxidize organics at the anode. 7

Figure 2. Layers within a typical gas diffusion electrode in a microbial peroxide producing cell. 9

Figure 3. Layers within ELAT2400 carbon-based gas diffusion electrode. 12

Figure 4. Expanded 3D model of electrochemical cell. 16

Figure 5. Calibration curve for the spectrophotometric determination of H_2O_2. 21

Figure 6. (a) H_2O_2 concentrations and **(b)** cathodic coulombic efficiencies for four different electrocatalyst loadings at a current density of **1 mA/cm^2**. Error bars represent standard error for quadruplicate trials. 25

Figure 7. **(a)** H_2O_2 concentrations and **(b)** cathodic coulombic efficiencies for four different electrocatalyst loadings at a current density of **0.5 mA/cm^2**. Error bars represent standard error for quadruplicate trials. 27

Figure 8. (a) H_2O_2 concentrations and **(b)** cathodic coulombic efficiencies for four different electrocatalyst loadings at a current density of **5 mA/cm^2**. Error bars represent standard error for quadruplicate trials. 30

Figure 9. (a) H_2O_2 concentrations and **(b)** cathodic coulombic efficiencies for four different electrocatalyst loadings at a current density of **9 mA/cm^2**. Error bars represent standard error for quadruplicate trials. 31

Figure 10. Linear sweep voltammograms of the 0.5, 1.5, 3.0, 5.0 mg/cm^2 cathodes and control at room temperature and an ionic strength of 100 mM. 34

Figure 11. Cross-sectional SEM images of different electrocatalyst loadings at magnification of 100X: **(a)** control, **(b)** 0.5 mg/cm^2, **(c)** 1.5 mg/cm^2, **(d)** 3.0 mg/cm^2, **(e)** 5.0 mg/cm^2. The side coated with carbon ink is at the top of the photo with green arrows indicating the thickness of the electrocatalyst layer. The images were created using the S4800 SEM at the Clemson University Electron Microscopy Lab. 38

List of Figures (continued)

Page

Figure 12. Cross-sectional SEM images of different electrocatalyst loadings at magnification of 150X: **(a)** control, **(b)** 0.5 mg/cm^2, **(c)** 1.5 mg/cm^2, **(d)** 3.0 mg/cm^2, **(e)** 5.0 mg/cm^2. The side coated with carbon ink is at the top of the photo with green arrows indicating the thickness of the electrocatalyst layer. The images were created using the S4800 SEM at the Clemson University Electron Microscopy Lab. 39

Figure 13. (a) H_2O_2 concentrations and **(b)** cathodic coulombic efficiencies for two electrocatalyst loadings with and without Nafion at a current density of **1 mA/cm^2**. Error bars represent standard error for quadruplicate trials. 41

Figure 14. Schematic diagram of proton hopping mechanism with Nafion. 42

Figure 15. Cross-sectional SEM images of electrocatalyst loadings without Nafion at a magnification of 100X: **(a)** 1.5 mg/cm^2, **(b)** 5.0 mg/cm^2 and 150X: **(c)** 1.5 mg/cm^2, **(d)** 5.0 mg/cm^2. The side coated with carbon ink is at the top of the photo with a green overlay encompassing the thickness of the MPL and electrocatalyst layer. The images were created using the S4800 SEM at the Clemson University Electron Microscopy Lab. 44

Figure 16. **(a)** H_2O_2 concentrations and **(b)** cathodic coulombic efficiencies for two PTFE/CB mass ratios with and without Nafion at a current density of **1 mA/cm^2** and electrocatalyst loading of **1.5 mg/cm^2**. Error bars represent standard error for quadruplicate trials. 46

Figure A-1. Configuration for H_2O_2 production experiments with electrodes connected to potentiostat and a recirculation line through the cathode chamber. 53

Figure A-2. Electrocatalyst ink and cathode preparation: **(a)** Vulcan XC 72 carbon powder, **(b)** carbon based electrocatalyst ink, **(c)** ELAT2400 bare cloth, **(d)** ELAT2400 painted with electrocatalyst. 53

Figure C-1. Average final cathode pH from electrocatalyst loading experiments. Error bars represent standard error for quadruplicate trials. 56

Figure C-2. Average final cathode pH from electrocatalyst ink composition experiments for **(a)** two electrocatalyst loadings with two different inks and **(b)** two PTFE/CB mass ratios with two different inks and an electrocatalyst loading of **1.5 mg/cm^2**. Error bars represent standard error for quadruplicate trials. 57

List of Figures (continued)

Page

Figure D-1. Cross-sectional SEM images of different electrocatalyst loadings at magnification of 220X: **(a)** control, **(b)** 0.5 mg/cm^2, **(c)** 1.5 mg/cm^2, **(d)** 3.0 mg/cm^2, **(e)** 5.0 mg/cm^2. The side coated with carbon ink is at the top of the photo with green arrows indicating the thickness of the electrocatalyst layer. The images were created using the S4800 SEM at the Clemson University Electron Microscopy Lab. 58

LIST OF SYMBOLS AND ABBREVIATIONS

AEM	Anion exchange membrane
Ag/AgCl	Silver/Silver Chloride
AO	Anthraquinone oxidation
AOP	Advanced oxidation process
BOD	Biochemical oxidation demand
CB	Carbon black
CCE	Cathodic coulombic efficiency
CEM	Cation exchange membrane
CI	Current interrupt
COD	Chemical oxygen demand
CoPc	Cobalt (II) phthalocyanine
CP	Chronopotentiometry
DDI	Distilled deionized
EAOP	Electrochemical advanced oxidation process
EF	Electro-Fenton
F	Faraday's constant
FO	Fenton's oxidation
GDE	Gas diffusion electrode
GDL	Gas diffusion layer
H_2O_2	Hydrogen peroxide
HAA	Haloacetic acid

List of Symbols and Abbreviations (continued)

HO_2^-	Hydroperoxide anion
I	Current
IEM	Ion exchange membrane
LSV	Linear sweep voltammetry
MFC	Microbial fuel cell
MPL	Microporous layer
MPPC	Microbial peroxide producing cell
Na_2HPO_4	Sodium phosphate dibasic anhydrous
$NaH_2PO_4 \cdot H_2O$	Sodium phosphate monobasic monohydrate
O_2	Oxygen gas
O_3	Ozone
OH•	Hydroxyl radical
ORR	Oxygen reduction reaction
PBS	Phosphate buffer solution
PTFE	Polytetrafluoroethylene
SEM	Scanning electron microscope
SHE	Standard hydrogen electrode
THM	Trihalomethane
UV	Ultraviolet
V	Cathode volume
$\eta_{cathode}$	Cathodic efficiency

1.0 INTRODUCTION

Hydrogen peroxide (H_2O_2) is a strong oxidant and disinfectant that offers high value to the water treatment industry. Many water treatment processes have the disadvantage of forming by-products. Electrochemical water treatment processes in particular can form undesirable chlorinated by-products, including trihalomethanes (THMs) and haloacetic acids (HAAs).[1, 2] H_2O_2 decomposes to only water and oxygen, making it an appealing chemical for the advanced oxidation of organic contaminants and disinfection of wastewater.[3] Traditional production methods to synthesize highly concentrated H_2O_2 present serious challenges due to high energy costs and risks in storage and transportation.[4] The in-situ electrosynthesis of H_2O_2 from the reduction of O_2 provides a more sustainable alternative production method. Electrosynthesis of H_2O_2 can be accomplished using a gas diffusion electrode (GDE), generating low concentrations of H_2O_2, acceptable for many water and wastewater treatment processes.

One example of an electrochemical process, wherein H_2O_2 could be generated, is the microbial fuel cell (MFC). Within a MFC, wastewater organics are oxidized at the anode, lowering the chemical oxygen demand (COD), while simultaneously converting energy contained in wastewater into electric current. As a variation of the traditional MFC, in a microbial peroxide producing cell (MPPC), the anodic oxidation of wastewater provides the necessary electrons for reduction of O_2 to H_2O_2 instead of H_2O at the cathode. A carbon-based GDE including an electrocatalyst loading is employed as the cathode in an effort to yield higher H_2O_2 concentrations. Once H_2O_2 is electrosynthesized, it can then produce hydroxyl radicals (OH•), which are critical for

advanced oxidation processes (AOPs) and electrochemical advanced oxidation processes (EAOPs), capable of removing recalcitrant organics from wastewater.

Optimizing the H_2O_2 concentrations synthesized in a MPPC while minimizing energy requirements is important to further the use of MPPCs in water and wastewater treatment applications. Previous studies have examined the effect of electrocatalyst loading on GDEs, however, the research presented here focuses on the impact of loading on the modification and thickness of the electrocatalyst layer on GDEs. This research examines how key parameters, such as electrocatalyst loading, electrocatalyst composition, hydrophobicity of the cathode surface, and current density, alter H_2O_2 production efficiencies.

2.0 BACKGROUND

2.1 Industrial Production and Applications

Hydrogen peroxide has a history as a chemical oxidant and disinfectant in a variety of industries, such as textiles, chemical synthesis, and medical disinfection.[4, 5] Considered a "green" chemical, H_2O_2 degrades only to water and oxygen, making it a sustainable choice for industrial use with its relatively low environmental impact. Large scale production of H_2O_2 is accomplished by the anthraquinone oxidation (AO) process. The AO process is beneficial in its production of H_2O_2, but is not considered an environmentally friendly method itself.[6] The inefficiency, high energy requirements, and production costs of the AO process have led researchers to focus on alternative production methods for H_2O_2.[4] Methods which produce H_2O_2 onsite have potential to avoid the safety and economic concerns with the transportation and storage of highly concentrated H_2O_2.[7]

H_2O_2 has especially been valuable in the water treatment industry, as it is a strong oxidant, which can decompose into hydroxyl radicals and oxygen, without producing any harmful by-products. In the paper and pulp industry, bleaching effluents for the elimination of color-producing compounds is challenging as it requires extensive treatment and cost. Biological treatment of the effluents removes a significant portion of the biochemical oxidation demand (BOD), but is ineffective in removing the nonbiodegradable organic material. Concentrated H_2O_2 provides a solution to this challenge with its strong oxidation potential and stable nature. When coupled with

ultraviolet (UV) disinfection, photolysis of H_2O_2 produces OH•, capable of oxidizing significant quantities of chemical products as an AOP:[8]

$$H_2O_2[+UV] \rightarrow 2OH\bullet \qquad \textbf{Eq. 1}$$

The UV-H_2O_2 process has also found success in the degradation of dye pollutants in the textile industry. Its use in this capacity includes the major advantage of no sludge formation.[9] In addition to UV-H_2O_2 treatment, another AOP is ozone (O_3) coupled with H_2O_2:

$$O_3 + H_2O_2 \rightarrow OH\bullet + O_2 + HO_2^- \qquad \textbf{Eq. 2}$$

Treatment by Fenton's oxidation (FO) is an AOP using Fenton's reagents: Fe^{2+} and H_2O_2. The iron acts as a catalyst to form hydroxyl radicals from H_2O_2. **Equation 3** is known as the classical Fenton's reaction equation:[10]

$$Fe^{2+} + H_2O_2 \rightarrow Fe^{3+} + OH^- + OH\bullet \qquad \textbf{Eq. 3}$$

The hydroxyl radicals can then act as oxidants in removing recalcitrant organic matter from wastewater or leachate. Fenton's treatment of leachate has demonstrated success with reduction of COD in the range of 35-90%.[10] The in-situ concentration of H_2O_2 can be used for disinfection or in an EAOP to also remove recalcitrant organics from wastewater. Electrochemical methods with H_2O_2 have become increasingly of interest as they are capable of treating wastewater with high toxicity and low biodegradability.[11] When coupled with a current and electrodes, FO is known as Electro-Fenton (EF) oxidation. The traditional methods of EF treatment add Fe^{2+} and H_2O_2 to the reaction externally with an inert electrode or adding only H_2O_2 from the outside and producing Fe^{2+} electrochemically from a sacrificial iron anode. A recent development in EF

treatment introduces a third technique with a GDE for in-situ electrogeneration of H_2O_2 at the cathode. The GDE reduces oxygen to H_2O_2 by a two-electron transfer:[12]

$$O_2 + 2H^+ + 2e^- \rightarrow H_2O_2 \qquad \textbf{Eq. 4}$$

An advantage of the in-situ production of H_2O_2 in EF is minimizing the risk related to transport, storage, and handling of the chemical. EF can also produce the oxidizing agents from both the cathode and anode, which is known as paired electrocatalysis, unlike traditional FO.[13] Additional advantages of the EF process with H_2O_2 include low energy requirements, no vapor emissions, and high treatment efficiency.[12]

2.2 Microbial Fuel Cells

Fuel cells are another convenient technology to synthesize H_2O_2 electrochemically. Fuel cells contain cathode and anode chambers, physically separated by an ion exchange membrane (IEM). Oxidation occurs in the anode chamber while reduction occurs simultaneously in the cathode chamber. A microbial fuel cell utilizes microorganisms to drive the oxidation reaction in the anode chamber. Microbes can oxidize small organic molecules, such as acetate, to generate electrons and protons, according to the following reaction:[14]

$$CH_3COO^- + 4H_2O \rightarrow 2HCO_3^- + 9H^+ + 8e^- \quad (E°' = -0.28\ V_{SHE}) \qquad \textbf{Eq. 5}$$

The electrons produced in the anode flow to the cathode through an external circuit. At the cathode, the electrons then take part in a reduction reaction.[4] For the production of H_2O_2, the Oxygen Reduction Reaction (ORR) is important. ORR occurs either in the $4e^-$ or $2e^-$ mechanism. The $4e^-$ ORR results from reduction of oxygen in the presence of precious metal electrocatalysts:[3]

$$O_2 + 2H_2O + 4e^- \rightarrow 4OH^- \quad (E^{\circ\prime} = +0.81\ V_{SHE}) \qquad \textbf{Eq. 6}$$

MFCs can convert organic matter to electricity directly.[15] Simultaneously, the organic matter is decomposed to CO_2, cleaning the wastewater in the process. There are advantages to MFCs when compared to technologies used for a similar purpose. When an air-cathode is used in an MFC, energy is not required for aeration as O_2 can pass through freely to the cathode surface. MFCs also have flexibility in terms of operating temperature, where they can operate efficiently at ambient and low temperatures. Since off-gases emitted from MFCs consist mostly of CO_2, gas treatment is not required. Lastly, with widespread application and even in locations with minimal electrical infrastructure, MFCs could be a suitable option.[16]

2.3 Microbial Peroxide Producing Cells

A type of MFC that supports the production of H_2O_2 is a microbial peroxide producing cell. At the cathode in MPPCs, oxygen is partially reduced ($2e^-$ mechanism) to H_2O_2, using a carbon electrocatalyst, contrary to a metal electrocatalyst for the $4e^-$ ORR:[3]

$$O_2 + 2H_2O + 2e^- \rightarrow H_2O_2 + 2OH^- \quad (E^{\circ\prime} = +0.28\ V_{SHE}) \quad pH < 11.8 \qquad \textbf{Eq. 7a}$$

$$O_2 + H_2O + 2e^- \rightarrow HO_2^- + OH^- \quad (E^{\circ\prime} = +0.28\ V_{SHE}) \quad pH > 11.8 \qquad \textbf{Eq. 7b}$$

A typical MPPC set-up used for electrosynthesis of H_2O_2 is shown in **Figure 1**. MPPC is a useful technology for wastewater treatment where microorganisms oxidize BOD at the anode and H_2O_2 is produced at the cathode, which can be used for disinfection in the final stages of treatment.[3]

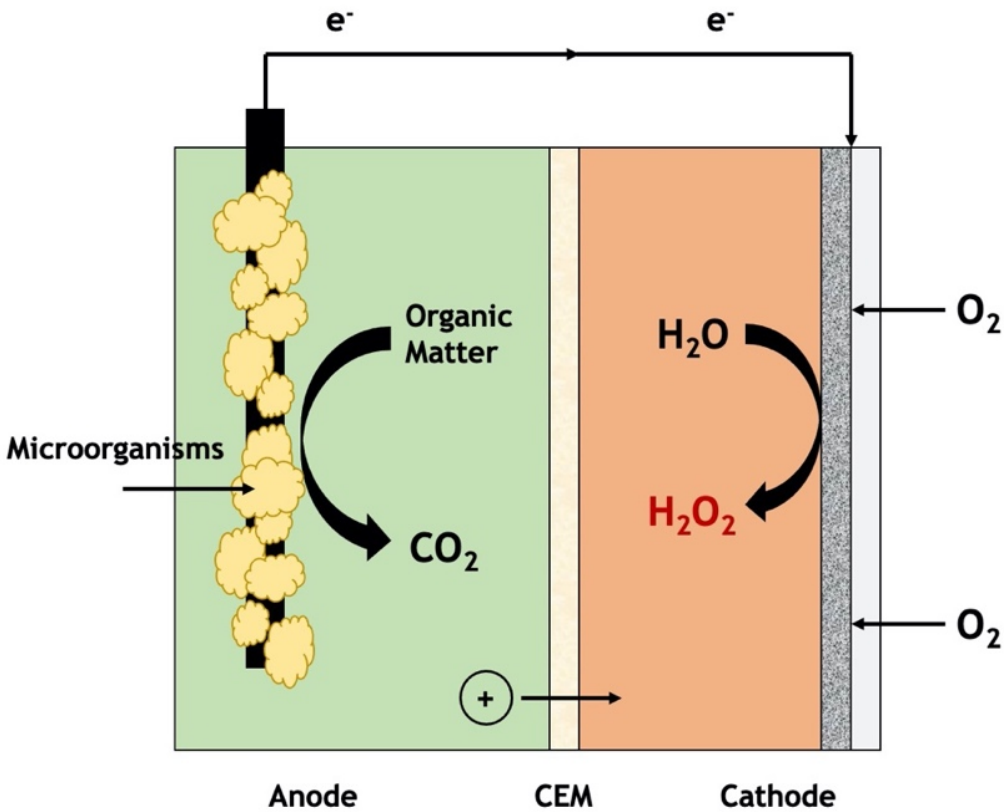

Figure 1. Schematic of MPPC which reduces oxygen to H_2O_2 at the cathode with bacteria to oxidize organics at the anode.

Maximum total voltage available from a fuel cell is calculated according to:

$$E_{cell} = E_{cathode} - E_{anode} \qquad \textbf{Eq. 8}$$

A MPPC with the $2e^-$ ORR at either pH condition (**Equation 7a** and **7b**) combined with the anode reaction (**Equation 5**) will have a maximum theoretical voltage of 0.56 V. This is a lower voltage than that achieved with the $4e^-$ ORR (1.1 V), but the production of H_2O_2 is an added benefit.

The cathodic coulombic efficiency (CCE) is used to evaluate the performance in terms of H_2O_2 production in MPPCs. Higher efficiencies correlate with higher H_2O_2 concentrations, which are needed for a successful MPPC and possible treatment. The

CCE quantifies the percentage of electrons used to reduce oxygen to H_2O_2. The CCE ($\eta_{cathode}$) is defined by **Equation 9**:[3]

$$\eta_{cathode} = ([H_2O_2]_{actual} / [H_2O_2]_{theoretical}) * 100\% \qquad \textbf{Eq. 9}$$

$$[H_2O_2]_{theoretical} = \frac{I}{F} * \frac{HRT}{V} * \frac{3600\ s}{hr} * \frac{1\ mol\ H_2O_2}{2\ mol\ e^-}$$

where *I* is the current (mA), *F* is Faraday's constant (96485 $\frac{C}{mol\ e^-}$), *V* is the cathode volume (mL), and *HRT* is in hours. Cathodic efficiency is influenced by solution pH, electrode structure, ease of the ORR reaction, and catalyst[17]. A cathode demonstrating higher cathodic efficiency indicates more efficient H_2O_2 production.

2.4 Gas Diffusion Electrodes

One of the challenges for the electrogeneration of H_2O_2 is the low aqueous solubility of oxygen into the electrolyte solution.[18] One type of cathode implemented with a MPPC is a GDE. The GDE is a promising solution to this challenge of low oxygen solubility. With a porous hydrophobic structure, the GDE allows oxygen to directly pass through and enter the electrocatalyst at a three-phase boundary layer.[18, 19] This prevents the mass-transport limitation of the dissolution of oxygen into the electrolyte, while also promoting more efficient electrosynthesis of H_2O_2.[20] Furthermore, with an unlimited supply of oxygen allowed to pass through the porous structure of a GDE, there is no need to pump oxygen directly into the cell, which reduces operating costs.[19]

The layers within the GDE comprise a few hundred microns in thickness using a carbon cloth as the backbone. This carbon cloth acts as a current collector, carrying the electric current to and from the electrode.[19] Within the porous structure of the GDE, there is an active electrocatalyst layer and a gas diffusion layer (GDL). The electrocatalyst

layer faces the electrolyte, while a hydrophobic microporous layer (MPL) and carbon cloth together act as the GDL and face the air side. The oxygen gas must diffuse through the micropores of the GDL to reach the electrocatalyst layer and then react at the three-phase boundary layer (**Figure 2**). The electrocatalyst layer is usually implemented in an attempt to increase H_2O_2 production while reducing overpotentials. The GDL of a GDE is typically hydrophobic to promote gas transfer of oxygen through the micropores of the layer. The electrocatalyst layer needs a balance of both hydrophobic and hydrophilic properties because it lies between the diffusion layer and the electrolyte solution.[21]

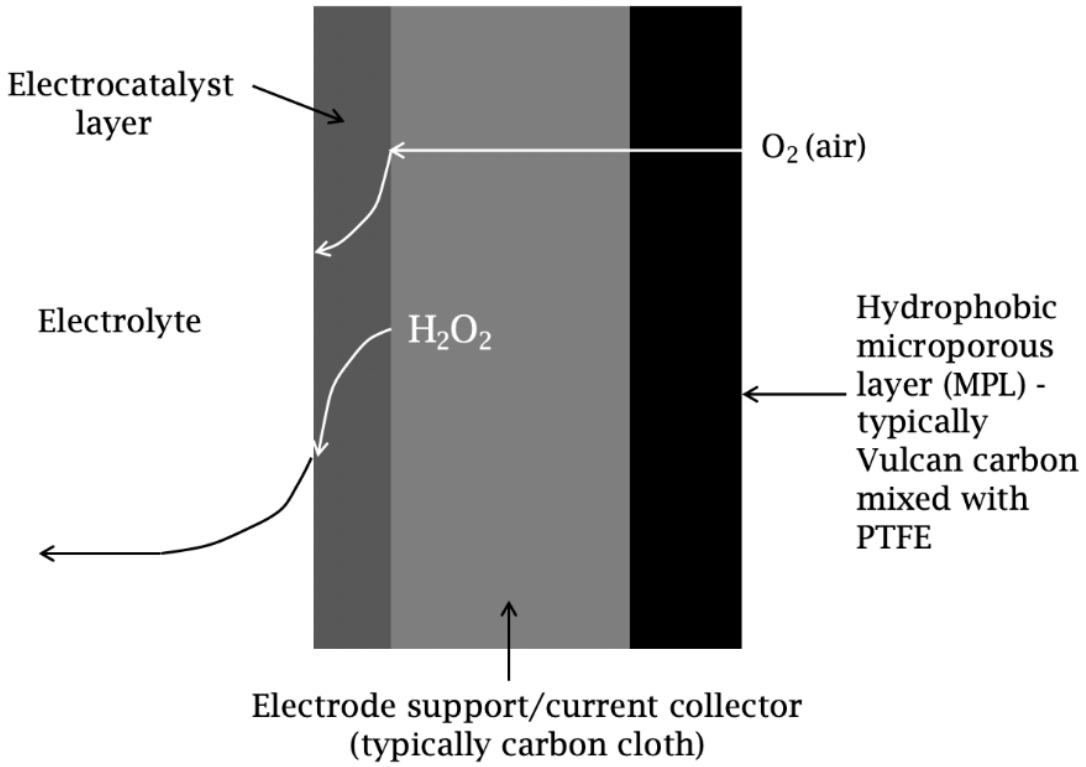

Figure 2. Layers within a typical gas diffusion electrode in a microbial peroxide producing cell.

2.5 Electrocatalysts

Research on GDEs has been directed towards improving O_2 mass transfer efficiency and addition of electrocatalyst to increase H_2O_2 production. Recent studies have experimented with altering the GDE through the addition of specific metals to act as electrocatalysts to promote the $2e^-$ ORR. Barros et al. modified a GDE with various amounts of cobalt (II) phthalocyanine (CoPc), which can reduce the potential for oxidation-reaction reactions. The addition of CoPc increased the H_2O_2 yield by 89.1% compared to a GDE with no CoPc coating.[22]

Polytetrafluoroethylene (PTFE) has also shown success when used in the electrocatalyst layer of a GDE. As a hydrophobic polymer, PTFE improves the porosity of the GDE, resulting in more channels for oxygen to reach the three-phase boundary and decreasing oxygen transport resistance. Ding et al. focused on the influence of PTFE on the microstructure of the GDE, observing an increase in hydrophobic behavior in the diffusion layers of the GDE with increasing PTFE content in the catalytic layer.[23] Yu et al. examined the effect of a carbon black (CB) and PTFE electrocatalyst on H_2O_2 production on a graphite electrode, discovering a mass ratio of 5:1 PTFE to CB increased H_2O_2 concentrations by 10.7 times.[18] When implemented at the ORR interface on a natural air diffusion electrode, Zhang et al. found optimum mass ratio of 0.6 PTFE to CB to achieve the greatest H_2O_2 concentrations.[20] The carbon-PTFE O_2-fed GDE used by Brillas et al. obtained the optimum H_2O_2 concentration of 59 $mg/cm^2/hr$ at a current density of 242 mA/cm^2. The structural integrity of the GDE diminished quickly and since pure oxygen was supplied to the electrochemical cell, only a small percentage of the

oxygen was utilized.[24] Research has focused on solving the oxygen supply issue with GDEs, where the oxygen utilization efficiency is very low.[20] Martinez et al. has demonstrated that a higher O_2 supply promotes H_2O_2 production, while simultaneously increasing the energy requirements of the system.[25]

2.6 Cathode Design

One type of GDE is that pictured in **Figure 2** where the GDL consists of the carbon cloth and MPL on one side of the cloth. The electrocatalyst ink is then applied on the side of the cloth with no MPL, expected to form an electrocatalyst layer on top of the GDL. Prior work has been done to determine an optimal electrocatalyst loading on this type of GDE made from CeTech Carbon Cloth with a MPL on one side of the cloth. The study discovered that instead of forming a distinct electrocatalyst layer, the ink was embedded into the pores of the carbon cloth, impacting the porosity of the GDL. An increase in electrocatalyst loading correlated with decreased porosity of the GDL, resulting in a more tortuous path for H_2O_2 to travel and diffuse into the electrolyte.[26] An ELAT1400 carbon cloth is also designed in the same way.

An alternative type of GDE is pictured in **Figure 3**, where the GDL encompasses the carbon cloth and two MPLs, one on each side of the cloth. The electrocatalyst is then applied on top of one of the MPLs. Carbon cloths of this kind include the ELAT2400. Further research was performed to compare the columbic efficiencies of the CeTech cathode to GDEs made from ELAT1400 and ELAT2400 carbon cloth with no electrocatalyst loading, with the last showing the highest efficiency.[27] The present research expands on the findings by using the ELAT2400 as the carbon-based cloth

material for the GDE to further examine the relationship between different electrocatalyst loadings and cathode architecture. For the ELAT2400 GDE, it is expected to see a distinct layer of electrocatalyst on the top of the MPL adding noticeable thickness to the diffusion pathway.

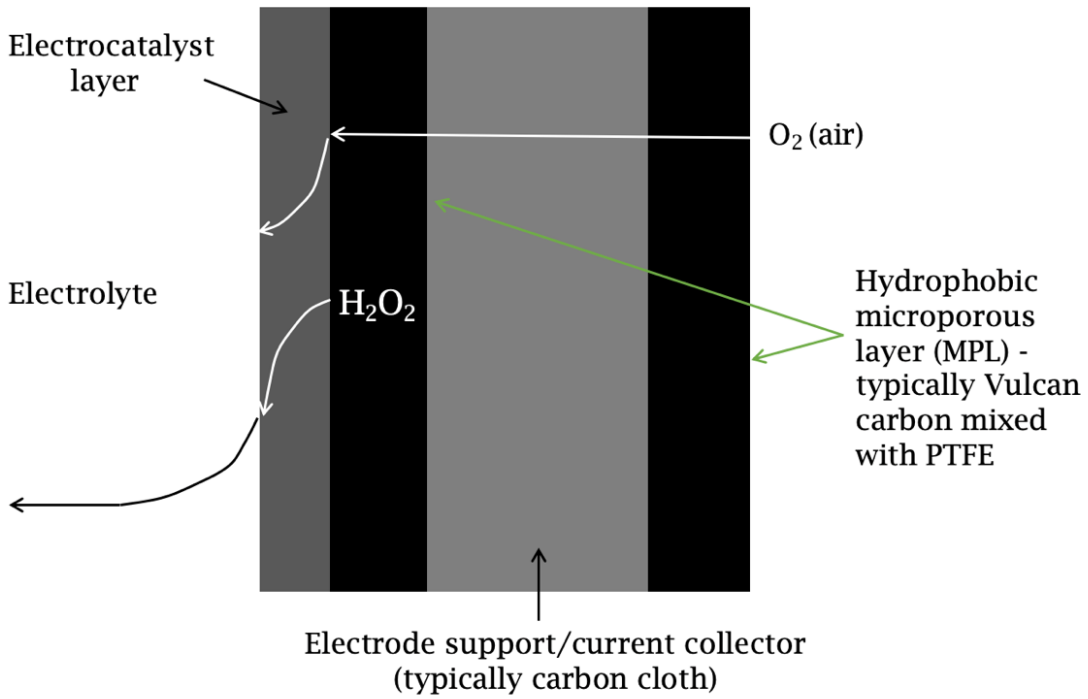

Figure 3. Layers within ELAT2400 carbon-based gas diffusion electrode.

The electrocatalyst ink composition typically uses Nafion dispersion, which is comprised of a mixture of ethanol, propanol, and Nafion polymer. In an effort to understand the impact of Nafion on mass transport in a GDE, this research uses carbon inks with and without Nafion in two different electrocatalyst ink compositions to compare their H_2O_2 productions. The two modifications to the GDE relating to the electrocatalyst loading and composition ultimately focus on improving the efficiency of a MPPC at the cathode.

3.0 RESEARCH OBJECTIVES

The scope of this thesis stems from the findings of a previous study by Murawski where the effect of electrocatalyst loading on gas diffusion electrodes was related to porosity and modification of the inner cathode structure. This prior work determined an optimal electrocatalyst loading on a GDE made from CeTech Carbon Cloth with a MPL on one side of the cloth.[26] By selecting the ELAT2400 as the GDE with two MPLs in the GDL on both sides of the cloth, the following research objectives were designed to answer the question, "How does the modification of electrocatalyst loading and composition impact the structure of the gas diffusion layer in a gas diffusion electrode for optimization of H_2O_2 production?"

Specifically, the objectives of this research are:

1. ***Determine the effect of electrocatalyst loading on H_2O_2 production.*** Cathodes with electrocatalyst loadings of 0.5, 1.5, 3.0, and 5.0 mg/cm^2 were tested for cathodic coulombic efficiencies by applying a constant current and measuring H_2O_2 concentrations over time. Current densities of 0.5, 1.0, 5.0, and 9.0 mA/cm^2 were applied to each cathode and H_2O_2 concentrations were measured over the reaction time period. As electrocatalyst loading is increased, it is hypothesized that the H_2O_2 production efficiencies will decrease due to increased electrode thickness.
2. ***Examine the relationship between electrocatalyst loading and cathode structure.*** Each electrocatalyst loading was imaged using a high resolution S4800 scanning electron microscope (SEM) at magnifications of 100X, 150X,

and 220X. It is hypothesized that the SEM images will show a distinct electrocatalyst layer on the electrode, with an increase in the layer thickness as loading is increased.

3. ***Determine the effect of electrocatalyst ink composition on H_2O_2 production***. Cathodes with electrocatalyst loadings of 1.5 mg/cm^2 and 5.0 mg/cm^2 made from carbon inks with and without Nafion were tested for cathodic coulombic efficiencies and produced H_2O_2 concentrations. Cathodes with electrocatalyst loading of 1.5 mg/cm^2 with carbon inks containing mass ratios of 1.0 and 1.6 PTFE/CB were also tested for cathodic coulombic efficiencies and produced H_2O_2 concentrations. Without the presence of Nafion in the electrocatalyst, it is hypothesized that H_2O_2 production efficiencies will increase if Nafion is limiting the mass transport of H_2O_2 through the electrocatalyst layer.

4.0 MATERIALS AND METHODS

4.1 Electrochemical Cell

Four identical electrochemical cells were constructed to perform the H_2O_2 production experiments, as seen in **Figure 4**. Plexiglas frames (10 cm x 10 cm) were used for the cathode and anode chambers, with 25 cm^2 hollowed centers that acted as the electrolyte chambers. The cathode plate was 1.3 cm thick and the anode plate was 0.6 cm thick. The volumes of the cathode and anode chambers were approximately 20 mL and 50 mL, respectively, but varied slightly for each experiment. The volumes of electrolyte in the two chambers were recorded for each experiment as the theoretical H_2O_2 that could be produced and the cathodic coulombic efficiency calculations are influenced by the volume of electrolyte in the cathode chamber. Silicone gaskets were placed in between each Plexiglas plate to avoid leaks. An additional Plexiglas plate with no hollowed center served as the back plate for the anode chamber. The cathode and anode chambers were separated by a 127 μm Chemours Nafion cation exchange membrane (CEM) to allow transport of ions and to reduce potential for H_2O_2 degradation. A CEM was selected instead of an anion exchange membrane (AEM) since CEMs are less susceptible to H_2O_2 degradation.[30] A stainless steel plate (10 cm x 10 cm) served as the current collector to evenly distribute the current, with a 25 cm^2 hollowed center for O_2 to diffuse through the cathode. Each Plexiglas plate, silicone gasket, and stainless steel plate had eight holes for insertion of eight screws and wingnuts to hold the cell together with a tight seal.

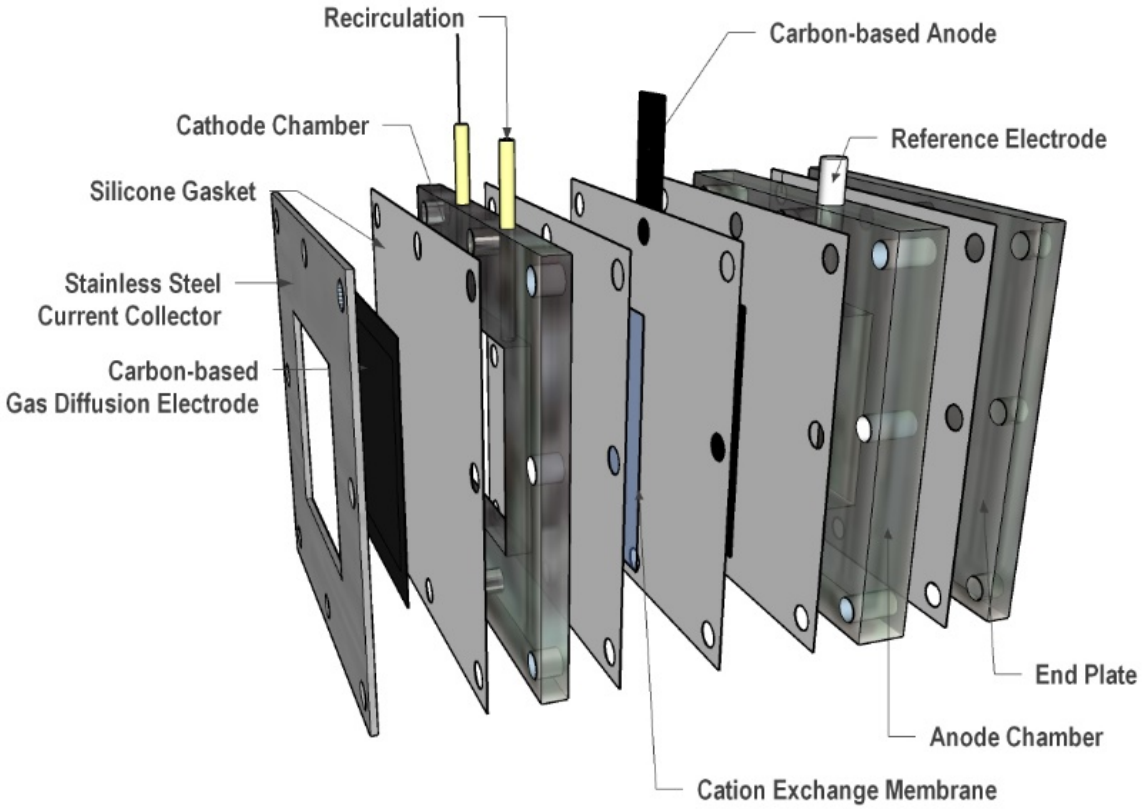

Figure 4. Expanded 3D model of electrochemical cell.[27]

The cathode was a GDE, made from an ELAT2400 carbon cloth with a hydrophobic MPL on each side and carbon electrocatalyst loading coated on one of the MPLs. The uncoated MPL was exposed to air to allow O_2 to diffuse into the cathode chamber and be reduced to H_2O_2. The electrocatalyst-coated layer of the cathode faced the CEM and electrolyte solution. The anode was a woven carbon cloth. Within the cathode and anode chambers was a 100 mM phosphate buffer solution (PBS), made from 32 mM sodium phosphate dibasic anhydrous (Na_2HPO_4) and 68 mM of sodium monobasic monohydrate ($NaH_2PO_4 \cdot H_2O$), with a pH of about 6.5-6.6. Two holes were drilled at the top of each chamber of the electrochemical cell. For the anode chamber, a

RE-5B Ag/AgCl reference electrode with flexible connector from Bioanalytical Systems, Inc. was inserted into one hole and the electrolyte solution was pumped into the chamber through the second hole with a Fisher Scientific FH100M multichannel peristaltic pump. The two holes in the cathode chamber allowed for a recirculation line to ensure adequate mixing of the electrolyte during the experiment. The electrolyte in the cathode chamber was recirculated at a rate of 60 mL/min, based off findings from work previously done by Lindsay.[27] The cathode, anode, and reference electrode were connected to a BioLogic VMP3 Multi-Channel Potentiostat to apply a current and monitor data as seen in **Figure A-1**.

4.2 Electrocatalyst Preparation

The electrocatalyst loading experiments used the same composition of Vulcan carbon electrocatalyst ink in different loadings. The carbon ink was prepared by adding 1 mL of distilled deionized (DDI) water and 5 mL of alcohol-based Nafion dispersion (1100 equivalent weight, 5% w/w) from Fuel Cell Store to 500 mg of Vulcan XC 72 carbon powder in a sterile scintillation vial. Physical and chemical properties of Vulcan XC 72 are provided in **Table B-1**. The ink was thoroughly mixed in an ultrasonic water bath for 30 minutes and allowed to stir with a magnetic stir bar for 24 hours before use. The ethanol-based electrocatalyst ink (without Nafion) was prepared in the same manner with 5 mL of 70% ethanol (BDH Chemicals) in place of the Nafion dispersion.

The PTFE experiments each used the same loading (1.5 mg/cm^2) of Vulcan carbon electrocatalyst ink with different ink compositions. A Nafion carbon ink with mass ratio of 1.6=PTFE/CB was prepared by adding 1 mL of DDI water, 0.5 mL of PTFE

(60 wt %), and 4.5 mL of Nafion dispersion to 500 mg of Vulcan XC 72 carbon powder in a sterile scintillation vial. Similarly, an ethanol carbon ink with mass ratio of 1.0=PTFE/CB was prepared by adding 1 mL of DDI water, 0.313 mL of PTFE, and 4.688 mL of 70% ethanol to 500 mg of Vulcan XC 72 carbon powder in a sterile scintillation vial. The mass ratios of PTFE/CB were selected based off findings in Zhang et al.[20] Both inks were thoroughly mixed in an ultrasonic water bath for 30 minutes and allowed to stir with a magnetic stir bar for 24 hours before use.

4.3 Cathode Preparation

For the cathode material, ELAT2400 carbon cloth was cut into 6.5 cm x 6.5 cm squares. The loadings determined the required volume of ink deposited onto the cloth. The following electrocatalyst loadings were applied in this study: 0.5 mg/cm^2, 1.5 mg/cm^2, 3.0 mg/cm^2, and 5.0 mg/cm^2 based off findings of work performed in Murawski.[26] To ensure the entire 25 cm^2 area exposed to the electrolyte had an even electrocatalyst loading, the ink was deposited in a 6 cm x 6 cm area on the middlemost portion of the cloth. The ink was pipetted onto the cloths in amounts of .216 mL, .648 mL, 1.296 mL, and 2.160 mL for the loadings of 0.5 mg/cm^2, 1.5 mg/cm^2, 3.0 mg/cm^2, and 5.0 mg/cm^2, respectively, and spread with a paintbrush for an even coating. The cathodes were allowed to air dry completely before being placed into the electrochemical cell. Each cathode with its specific loading was made in triplicate, two for H_2O_2 production experiments and one sample for GDE characterization.

4.4 Electrochemical Techniques

The experiments applied linear sweep voltammetry (LSV) and chronopotentiometry (CP) within the EC Lab® Software for insight into the electrochemical performance of GDEs. LSVs were performed before starting each H_2O_2 production experiment. There is resistance between the working electrode and reference electrode in a solution, resulting in an ohmic drop, which must be used to correct the measured potential of the GDE. The experimental results may vary greatly if the ohmic loss is not compensated for, with a possible significant difference between the applied potential and potential received by the cathode. The ZIR technique or current interrupt (CI) technique available on the BioLogic VMP3 Potentiostat was used to determine the ohmic drop in the electrochemical cell. The LSVs display polarization curves to show the differences in cathodic overpotential and voltage efficiency amongst the GDEs with different electrocatalyst loadings. LSVs were performed at a scan rate of 10 mV/s from a -0.6 V to 0.3 V potential range at 85% compensation. CP applies a constant current between the working and counter electrodes of the electrochemical cell where first, the ohmic loss is determined by the CI technique and the potential is measured at the working electrode over time.

4.5 H_2O_2 Production Experiments

H_2O_2 production experiments were performed after the LSVs. For each electrocatalyst loading, four currents (12.5 mA, 25 mA, 125 mA, and 225 mA representing current densities of 0.5 mA/cm^2, 1 mA/cm^2, 5 mA/cm^2, and 9 mA/cm^2) were applied to examine the effect of current density on H_2O_2 production and current

efficiency. For applied currents of 12.5 mA and 25.0 mA, H_2O_2 concentration was measured every 20 minutes over 2 hours. At 125.0 mA, H_2O_2 concentration was measured every 10 minutes over 1 hour and at 225.0 mA, H_2O_2 concentration was measured every 5 minutes over 30 minutes. To measure the H_2O_2 concentration at each time point, the pump was turned off and a tube removed from the cathode port for extraction of a sample. Approximately a 0.2 mL sample was extracted from the recirculation line in the cathode chamber into a 2 mL microcentrifuge tube. The cathode tubing was returned to its port and the pump turned back on until the next sampling. The exact volume extracted was recorded and the cumulative volume removed from sampling over the course of the experiment was calculated and accounted for in subsequent H_2O_2 concentration calculations. At a relatively small cathode volume of 20 mL, small changes in the electrolyte volume impact both the H_2O_2 concentration and cathodic efficiency. At the conclusion of each experiment, the pH of the anode and cathode chambers was measured using a Thermo Scientific Orion STAR A211 pH meter. The pH was measured to ensure proper functionality of the membrane and for potential analysis of a pH effect amongst the different loadings. **Figure C-1** and **C-2** show average final cathode pH values for each experiment. Each experiment was done in quadruplicate.

4.6 H_2O_2 Measurement

Measurements to determine the H_2O_2 concentrations were followed using the method described in Arends et al.[31] A 0.1 mL sample of known H_2O_2 concentration was added to 1 mL of titanium (IV) oxysulfate-sulfuric acid solution (27-31% H_2SO_4 basis) and 0.9 mL of DDI water in a 2 mL plastic cuvette and allowed to react for 10 minutes.

Then, the absorbance of the sample was read at a wavelength of 405 nm in a VWR UV-1600PC spectrophotometer. This was done for H_2O_2 concentrations of 0, 50, 100, 250, 500, 1000, 1500, and 2000 mg/L to create a standard curve of absorbance vs. H_2O_2 concentration, as seen in **Figure 5.** The higher the H_2O_2 concentration, the darker the yellow color develops in the cuvette, illustrated in the color gradient in **Figure A-3**. The same procedure was performed to determine the H_2O_2 concentration at each time point for the H_2O_2 production experiments. Then, the absorbance readings were compared to the standard curve of absorbance vs. H_2O_2 concentration. H_2O_2 may exist in the sample as both its protonated form and deprotonated form, the hydroperoxide anion (HO_2^-). An acidic reagent, the titanium (IV) oxysulfate-sulfuric acid solution ensures protonation of any HO_2^- present to provide an effective concentration including both species of H_2O_2 in the samples.

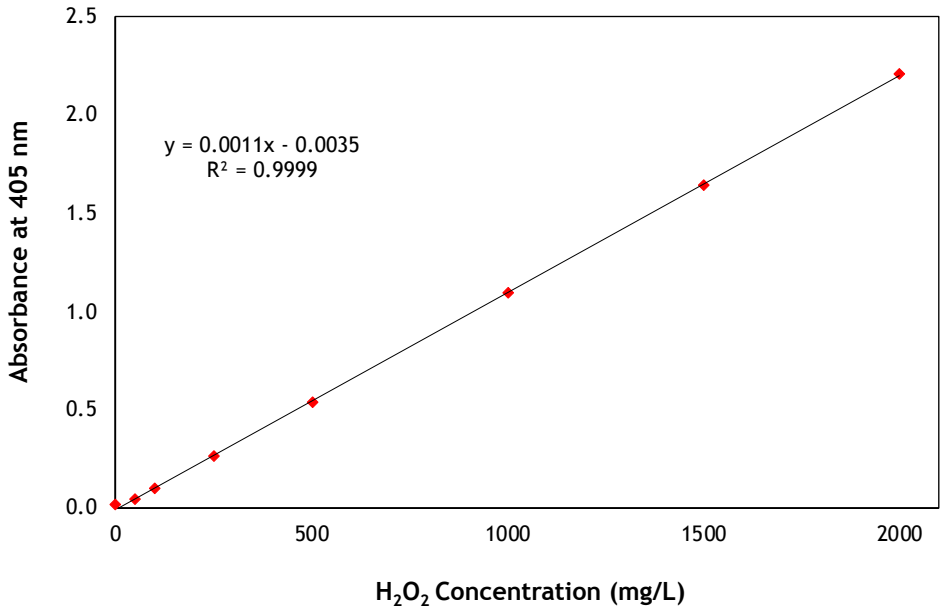

Figure 5. Calibration curve for the spectrophotometric determination of H_2O_2.

4.7 SEM Imaging

SEM was used for a visual understanding of the physical impact the different electrocatalyst loadings have on the electrode structure. Cross-sectional images of each cathode were imaged using a high resolution S4800 SEM at the Clemson University Electron Microscopy Laboratory. Samples of the carbon cloth cathodes (2 cm x 2 cm) coated with different electrocatalyst loadings were frozen in liquid nitrogen for about 10 minutes to provide a more solid structure to achieve a clean cut through the cloth fibers. The frozen cathode was then guillotine chopped with a razor blade at room temperature to obtain a smaller piece of material with the internal fibers of the cloth exposed. The chopped sample was mounted in a specimen stub with the sliced edge oriented towards the electron beam.[26] Each sample was imaged at 100X, 150X, and 220X.

5.0 RESULTS AND DISCUSSION

5.1 Effect of Electrocatalyst Loading on H_2O_2 Production

Lower electrocatalyst loadings on gas diffusion electrodes produced higher H_2O_2 concentrations with higher cathodic coulombic efficiencies, shown in **Figure 6**. A negative correlation is clear between electrocatalyst loading and H_2O_2 produced as the H_2O_2 concentrations increased with decreased loadings. The cathode with the lowest electrocatalyst loading of 0.5 mg/cm^2 performed optimally at a current density of 1 mA/cm^2, resulting in production efficiencies of 45-55%, whereas the highest loading of 5.0 mg/cm^2 produced the lowest concentrations of H_2O_2 and had efficiencies ranging from 5-15%.

When an electrocatalyst ink is deposited onto the porous side of a GDE with a MPL on the alternate side, the electrocatalyst is able to seep through the entire thickness of the cloth. On the contrary, the ELAT2400 electrode used in this study contains two MPLs, with the electrocatalyst ink deposited on one of them. The MPL restricts the ink from entering into the porous structure of the electrode, producing a distinguishable electrocatalyst layer sitting atop the MPL. An increased electrocatalyst loading corresponds to a thicker electrocatalyst layer, increasing the path required for H_2O_2 to diffuse into the electrolyte solution. The reduction of H_2O_2 from O_2 is only step 1 of a two-part mechanism. Once H_2O_2 is produced at the cathode, it may be further reduced to water in step 2 of the mechanism ($H_2O_2 + 2H^+ + 2e^- \rightarrow 2H_2O$).[28, 32] GDEs with higher electrocatalyst loadings, corresponding to greater thicknesses of the electrocatalyst layer, provide more sites for H_2O_2 to be reduced to water before it can reach the electrolyte

solution. Furthermore, water and oxygen can be produced when H_2O_2 reacts with itself ($2H_2O_2 \rightarrow 2H_2O + O_2$).[28] Therefore, in GDEs with longer diffusion pathways, it is more difficult for H_2O_2 to reach the electrolyte solution and lower H_2O_2 concentrations are produced. In GDEs with lower electrocatalyst loadings and therefore, smaller thicknesses of the electrocatalyst layer, the H_2O_2 is electrosynthesized at sites in the cathode closer to the electrolyte solution, with a shorter pathway to the electrolyte and lower probability of degradation.[28]

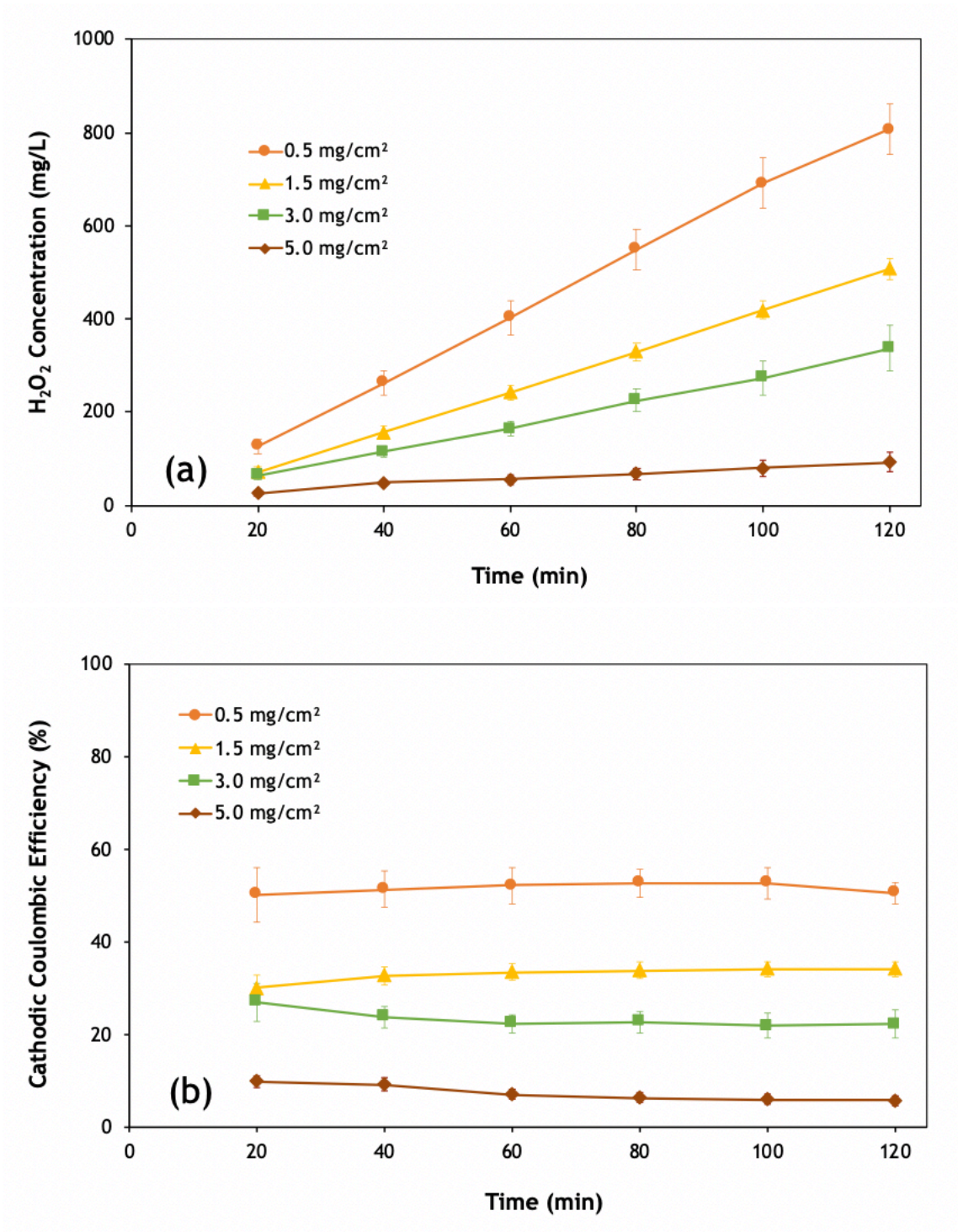

Figure 6. (a) H_2O_2 concentrations and **(b)** cathodic coulombic efficiencies for four different electrocatalyst loadings at a current density of **1 mA/cm²**. Error bars represent standard error for quadruplicate trials.

5.1.1 Effect of Current Density

The trends in **Figure 6** were also observed for electrocatalyst loadings across a range of current densities with their respective H_2O_2 concentrations increasing linearly with time. **Figure 7,** at an applied current density of 0.5 mA/cm^2, mimics the results from the 1 mA/cm^2 with the lowest loading producing the highest concentrations of H_2O_2. The efficiencies for each electrocatalyst loading also closely resemble those from the 1 mA/cm^2. The average maximum concentrations of H_2O_2 produced at 120 minutes for the 0.5 mg/cm^2 loading were 807.54 mg/L and 468.64 mg/L for current densities of 1.0 mA/cm^2 and 0.5 mA/cm^2, respectively. The remaining three loadings also produced about 40-60% less H_2O_2 at the lower 0.5 mA/cm^2 current density. This is logical since at lower applied current densities, fewer electrons are flowing to the cathode and are available for use to electrochemically reduce O_2 to H_2O_2.

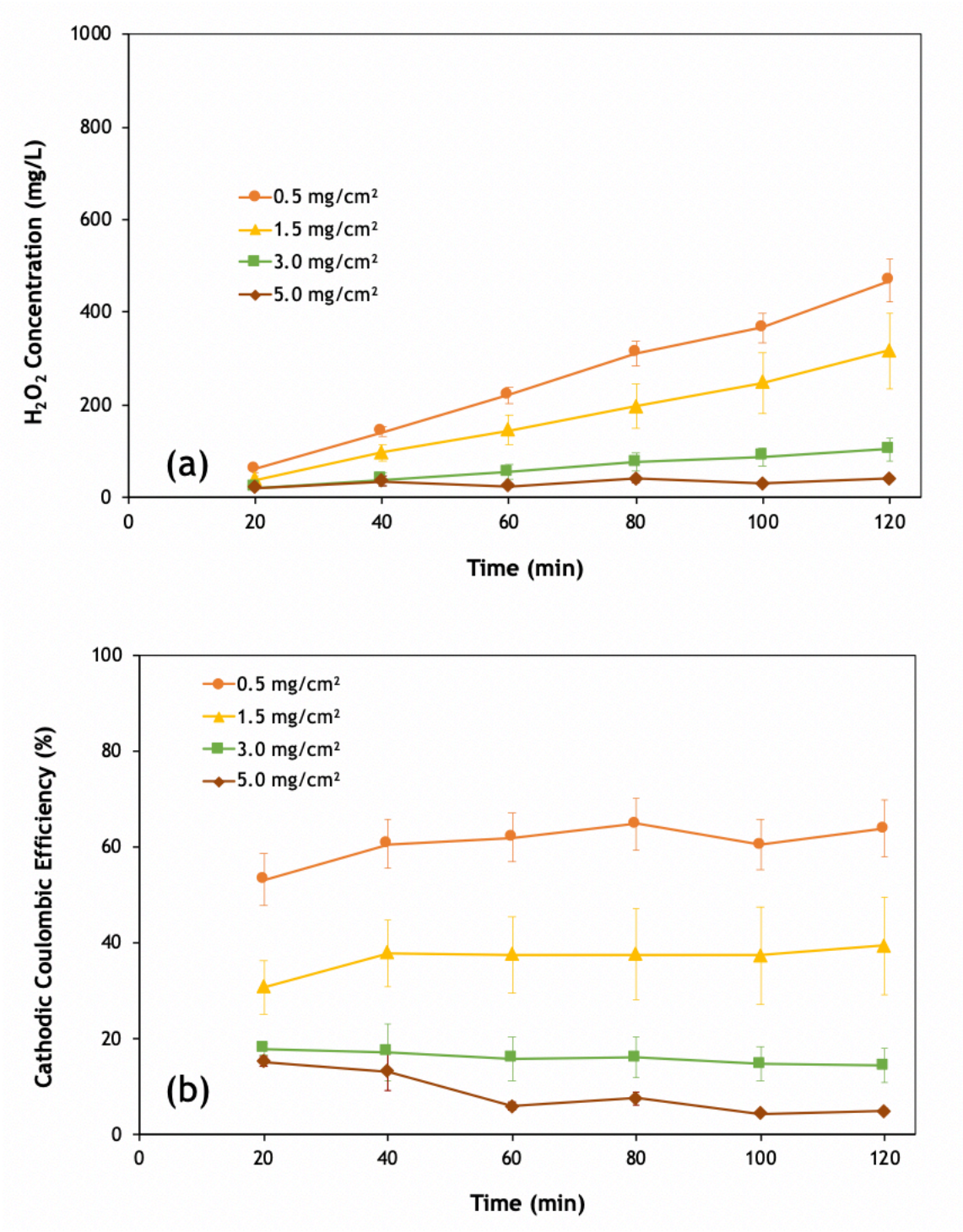

Figure 7. **(a)** H_2O_2 concentrations and **(b)** cathodic coulombic efficiencies for four different electrocatalyst loadings at a current density of **0.5 mA/cm^2**. Error bars represent standard error for quadruplicate trials.

The greatest differences between H_2O_2 production and CCE occur between the 1 mA/cm^2 and 5 mA/cm^2 applied current densities. **Figure 8** displays the results from the 5 mA/cm^2 current density for an experiment length of 60 minutes. Although the running time of the experiment was halved from the 0.5 mA/cm^2 and 1 mA/cm^2 current densities, the H_2O_2 concentrations at any given time point were much greater for the 5 mA/cm^2. The average maximum concentrations achieved after 60 minutes for the 0.5, 1.5, 3.0, and 5.0 mg/cm^2 loadings were 2008.79 mg/L, 1561.08 mg/L, 1714.63 mg/L, and 1553.58 mg/L, respectively. At a higher current density, the differences in produced H_2O_2 are diminished as the data points for the higher loadings close in on that of the lower loadings, as seen in **Figure 8a** and **8b**. The lines depicting H_2O_2 production at the different loadings for the 5 mA/cm^2 are closer together compared to the 1 mA/cm^2. The efficiencies follow this trend, as the 0.5 mg/cm^2 remains with average efficiencies in the range of 50-60% and the higher loadings improve their efficiencies while approaching the 0.5 mg/cm^2 line.

The same observation is echoed in the highest applied current density of 9 mA/cm^2 in **Figure 9**. Although the 3.0 mg/cm^2 loading produced slightly less H_2O_2 than the other loadings, all four lines experience significant overlap as comparable H_2O_2 concentrations are produced at every time point. Furthermore, the efficiencies of all loadings fall within the 45-65% range, with the highest loading of 5.0 mg/cm^2 improving the greatest from 5-15% at 0.5 mA/cm^2 to 45-50% at 9 mA/cm^2. Although H_2O_2 production increased with increasing current density for higher loadings, it is important to note that regardless of current density, the lowest loading of 0.5 mg/cm^2 produced

average efficiencies of 55-65%, indicating a smaller effect of current density on lower loadings.

There are two key factors influencing the H_2O_2 concentration measured in the electrolyte: how much H_2O_2 is formed from the reduction of O_2 and how much of the H_2O_2 is electrochemically reduced to water or chemically decomposed to O_2. From the aforementioned results, it is proposed that eventually both the formation and decomposition of H_2O_2 reach finite rates. An increase in current density showed improved performance by all electrocatalyst loadings, indicating a faster rate of formation of H_2O_2. With more electrons available for reduction at a higher current density, the rate of electrochemical reduction of H_2O_2 to H_2O is expected to increase as well. This would imply that the chemical decomposition rate stays similar across current densities and is more important at a lower current density where the formation rate is lower.

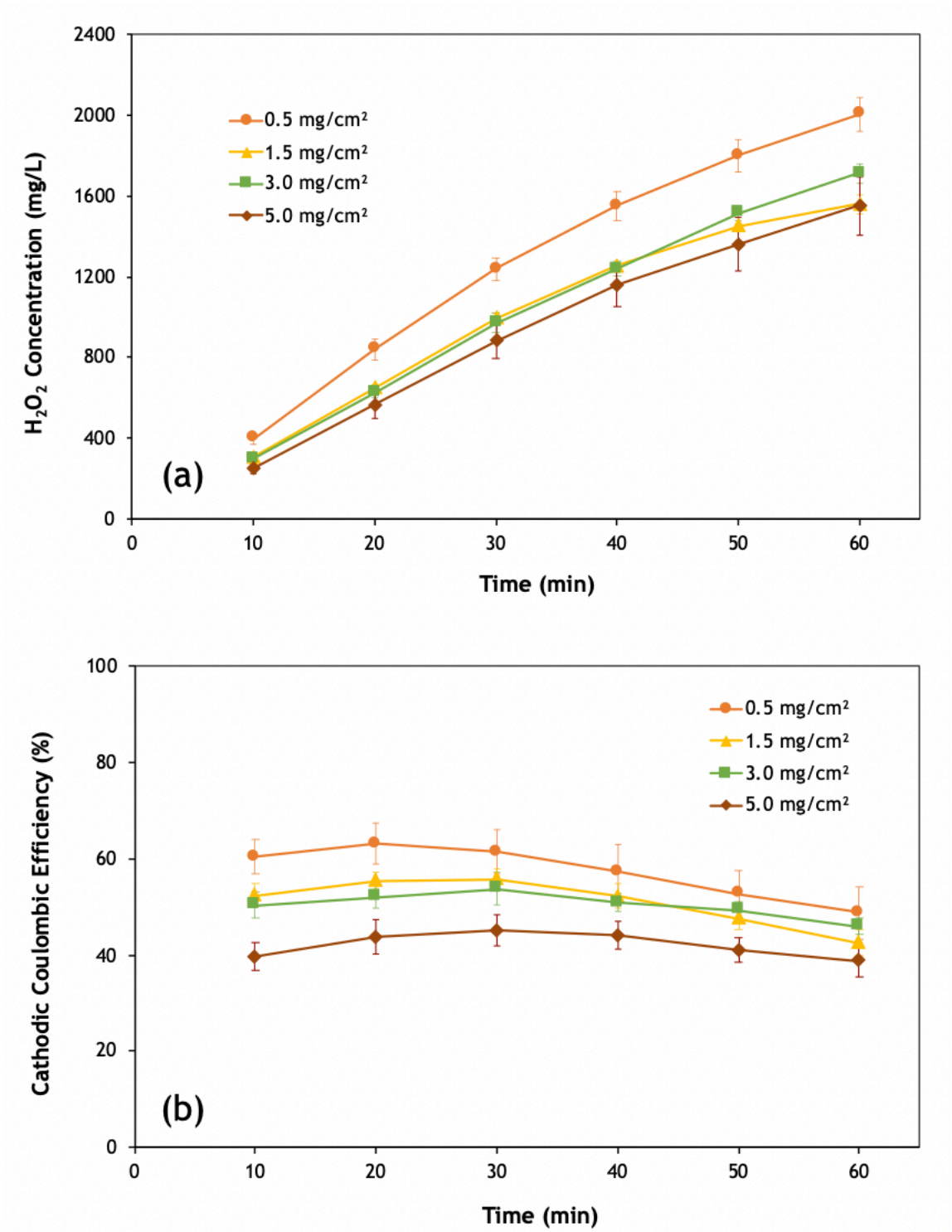

Figure 8. (**a**) H_2O_2 concentrations and **(b)** cathodic coulombic efficiencies for four different electrocatalyst loadings at a current density of **5 mA/cm²**. Error bars represent standard error for quadruplicate trials.

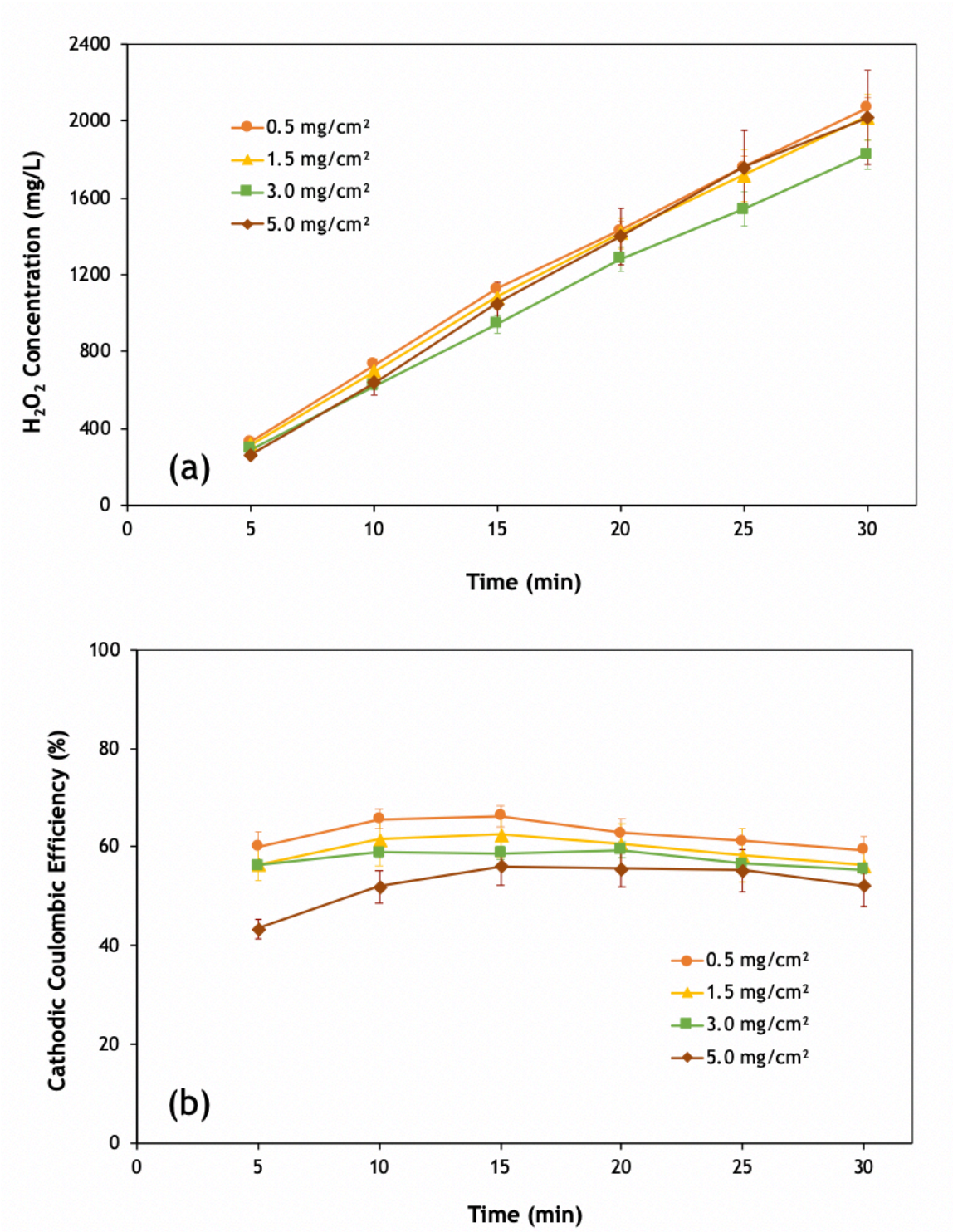

Figure 9. (a) H_2O_2 concentrations and **(b)** cathodic coulombic efficiencies for four different electrocatalyst loadings at a current density of **9 mA/cm²**. Error bars represent standard error for quadruplicate trials.

The results shown in **Figure 10** introduce an important consideration when selecting an electrocatalyst loading for H_2O_2 production in a MPPC. Based on the H_2O_2 concentrations and calculated efficiencies in the previous section, it would appear that the lower loadings are the best choices to improve electrosynthesis of H_2O_2. However, **Figure 10** displays LSVs for each of the cathodes and provides evidence that there are benefits to higher electrocatalyst loadings in terms of energy requirements. The $2e^-$ ORR has a theoretical potential of +0.32 V_{SHE} for the cathode reaction, indicated by the dashed line, with a theoretical potential of -0.26 V_{SHE} for the anode reaction, the dotted line. The cathode's overpotential is the difference between the theoretical potential of the cathode reaction and the potential of a selected cathode at a specified current density. As the cathodic overpotential increases, the external energy input required for the ORR to proceed also increases. A minimization of cathodic overpotential indicates an increase in voltage efficiency, which will require less external energy input to achieve a desired H_2O_2 concentration.

Comparison of the LSVs for the various electrocatalyst loadings indicates which loading is most favorable for the ORR reaction to proceed. External energy input is not necessary for cathodes with potentials that fall within the range of the theoretical potential for the anode and cathode (less than +0.32 V_{SHE} and greater than -0.26 V_{SHE}). This means that at lower current densities (0 to 3 mA/cm^2), the $2e^-$ ORR is favored to produce the theoretical H_2O_2 concentrations for the four different electrocatalyst loadings. As the current density increases, two important considerations arise. First, the cathodic overpotential increases for all electrocatalyst loadings and a greater external

energy input is required to produce an equivalent amount of H_2O_2 as at a lower current density. Second, at higher current densities, the potentials for the various electrocatalyst loadings are more spread apart, indicating a significantly larger overpotential for 0.5 mg/cm^2 compared to 5.0 mg/cm^2. Although the lowest loading of 0.5 mg/cm^2 produced the greatest amount of H_2O_2, it is worth considering a higher electrocatalyst loading at a higher current density to achieve a balance between external energy input and H_2O_2 produced. The control cathode with no electrocatalyst applied has the highest overpotential compared to the electrocatalyst loading cathodes and would require an external energy input at any current density. Therefore, regardless of the current density selected, addition of the electrocatalyst is justified.

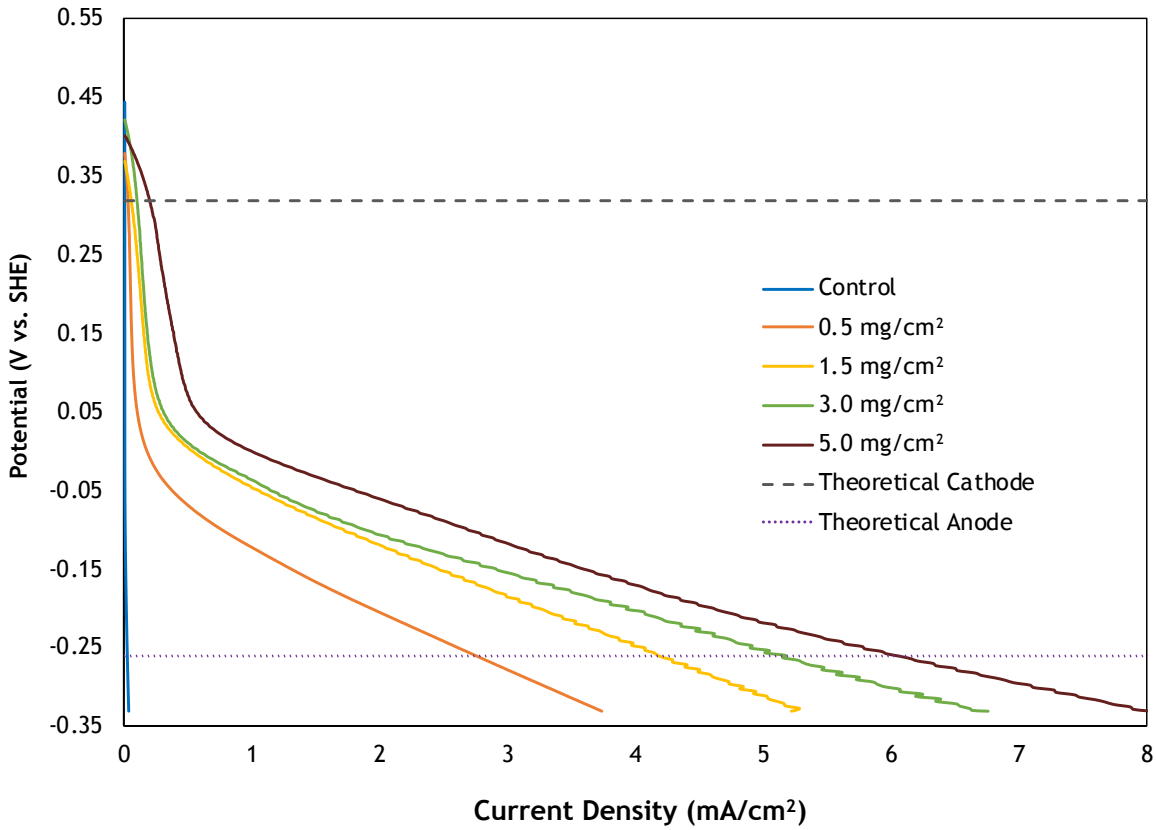

Figure 10. Linear sweep voltammograms of the 0.5, 1.5, 3.0, 5.0 mg/cm^2 cathodes and control at room temperature and an ionic strength of 100 mM.

5.1.2 Energy Input Analysis

The observations of the LSVs raise an important point, suggesting the optimum electrocatalyst loading selected may change depending on the applied current density. At higher current densities, especially 5 mA/cm^2 and greater, the LSVs clearly showed a higher loading to be more energy favored due to requiring significantly less energy input than a lower loading. In addition, since the H_2O_2 production results show that a higher loading of 5.0 mg/cm^2 can achieve similar concentrations as a cathode with 0.5 mg/cm^2 loading, it might make sense to select a higher electrocatalyst loading at higher current

densities. **Table 1** shows an energy input breakdown to compare the mass of H_2O_2 that can be produced per kWh for each electrocatalyst loading at two different current densities. A potential of -0.05 V was assumed for the anode. Since the potentials for electrocatalyst loadings of 1.5, 3.0, and 5.0 mg/cm^2 at 1.0 mA/cm^2 result in positive values for E_{cell}, no external energy input is required. It should also be noted that although at a current density of 5.0 mA/cm^2 there was no potential value for the electrocatalyst loading of 0.5 mg/cm^2, it would still require an external energy input. Considering results for the 5.0 mA/cm^2 current density, the mass of H_2O_2 produced per kWh inputted increases with electrocatalyst loading. This means that even though the lowest loading of 0.5 mg/cm^2 produced the highest concentrations of H_2O_2 at any given time point (**Figure 8**), the highest electrocatalyst loading of 5.0 mg/cm^2 is a better choice when energy is accounted for. This is especially true at a current density such as 5.0 mA/cm^2 and likely 9.0 mA/cm^2, where produced concentrations of H_2O_2 are fairly similar amongst the different loadings.

Table 1. Energy input comparison of H_2O_2 production at two current densities.

Current Density (mA/cm^2)	**Electrocatalyst Loading (mg/cm^2)**	**$E_{cathode}$ (V_{SHE})**	**E_{cell} (V_{SHE})**	**Mass Produced/Energy Input (kg H_2O_2/kWh)**
1	0.5	-0.124	-0.074	4.64
	1.5	-0.047	0.003	-
	3.0	-0.038	0.012	-
	5.0	-0.002	0.048	-
5	0.5	-	-	-
	1.5	-0.311	-0.261	2.68
	3.0	-0.253	-0.203	3.76
	5.0	-0.219	-0.169	3.84

5.2 Effect of Electrocatalyst Loading on Cathode Structure

5.2.1 SEM Images

As expected, the different loadings of electrocatalyst resulted in different thicknesses on top of the MPL that was coated with carbon ink. The SEM images in **Figure 11** show cross sections of the cathodes, each with a different electrocatalyst loading at a magnification of 100X. The identification of the carbon ink on the electrodes is indicated by a change in surface texture of the MPL. The bare carbon cloth without any addition of electrocatalyst ink, which acted as a control, has a rough surface, seen at the top of **Figure 11a**. When the carbon ink is painted onto the MPL, a smooth surface appears, shown in **Figure 11b-e** for the four different loadings. The thickness of the electrocatalyst layer on the cloth is indicated by the green arrows in each image.

SEM images at a closer magnification of 150X in **Figure 12** better define the differences in electrocatalyst layer thicknesses for the four loadings. Qualitatively, it is evident that the arrows lining the top and bottom of the electrocatalyst layer become further apart as the loading is increased, with 3.0 mg/cm^2 and 5.0 mg/cm^2 showing the most defined electrocatalyst layer. Since the MPL is still slightly porous, at lower loadings of 0.5 mg/cm^2 and 1.5 mg/cm^2, it is probable that the ink needs to fill any open pore spaces in the MPL before settling on top of the surface. Where the electrocatalyst layer is more defined at higher loadings, any pore spaces in the MPL must be occupied with ink and the remaining carbon ink lies on the top of the cathode. The increase in thickness of the electrocatalyst layer supports the results that lower amounts of H_2O_2 are produced with cathodes of higher electrocatalyst loadings. The thicker the electrocatalyst

layer, the greater the length of the perpendicular diffusion pathway required for H_2O_2 to travel to eventually diffuse into the electrolyte solution. H_2O_2 then has more electrocatalyst sites and a longer period of time to be electrochemically reduced to water or chemically decomposed back to O_2.

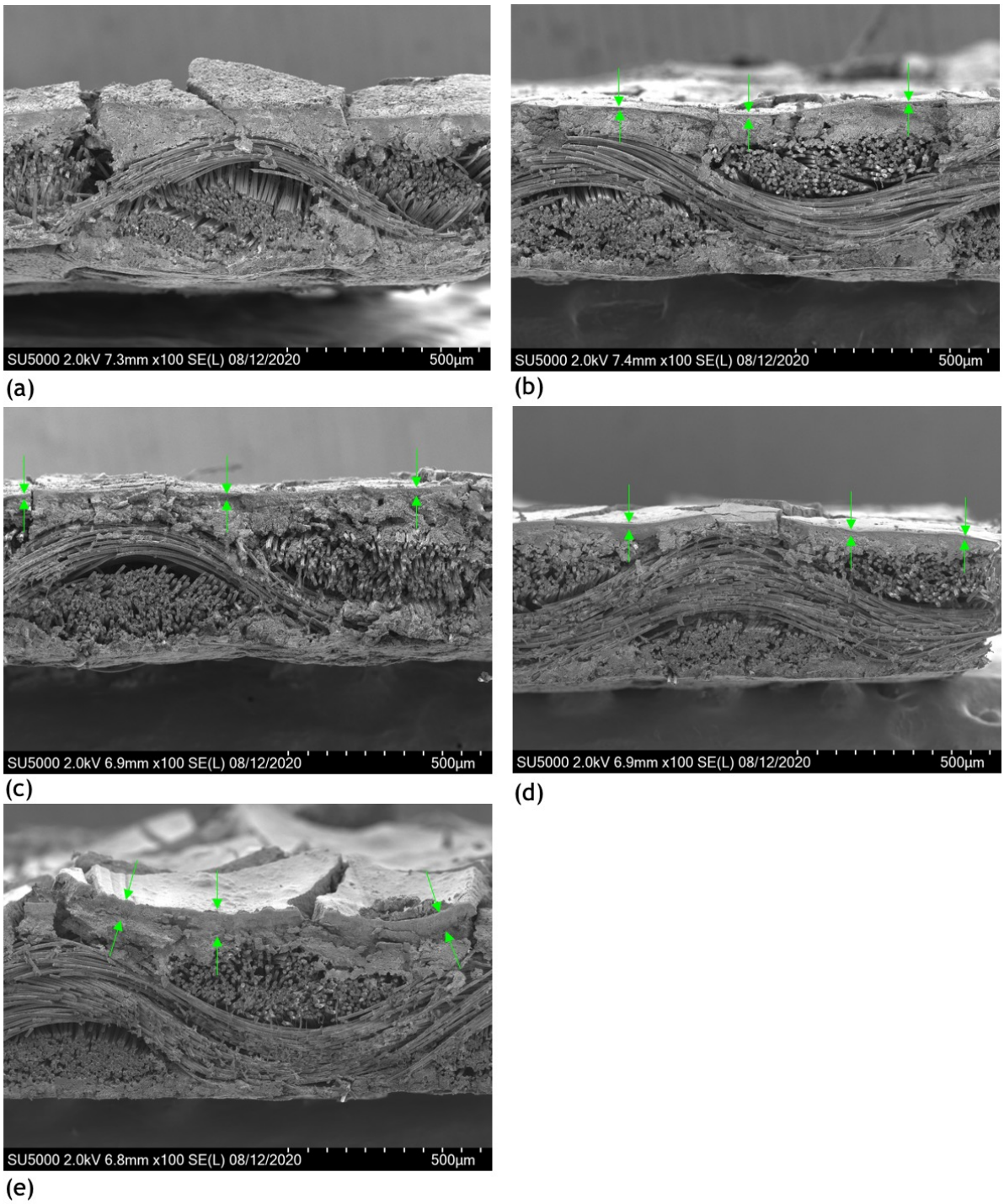

Figure 11. Cross-sectional SEM images of different electrocatalyst loadings at magnification of 100X: **(a)** control, **(b)** 0.5 mg/cm^2, **(c)** 1.5 mg/cm^2, **(d)** 3.0 mg/cm^2, **(e)** 5.0 mg/cm^2. The side coated with carbon ink is at the top of the photo with green arrows indicating the thickness of the electrocatalyst layer. The images were created using the S4800 SEM at the Clemson University Electron Microscopy Lab.

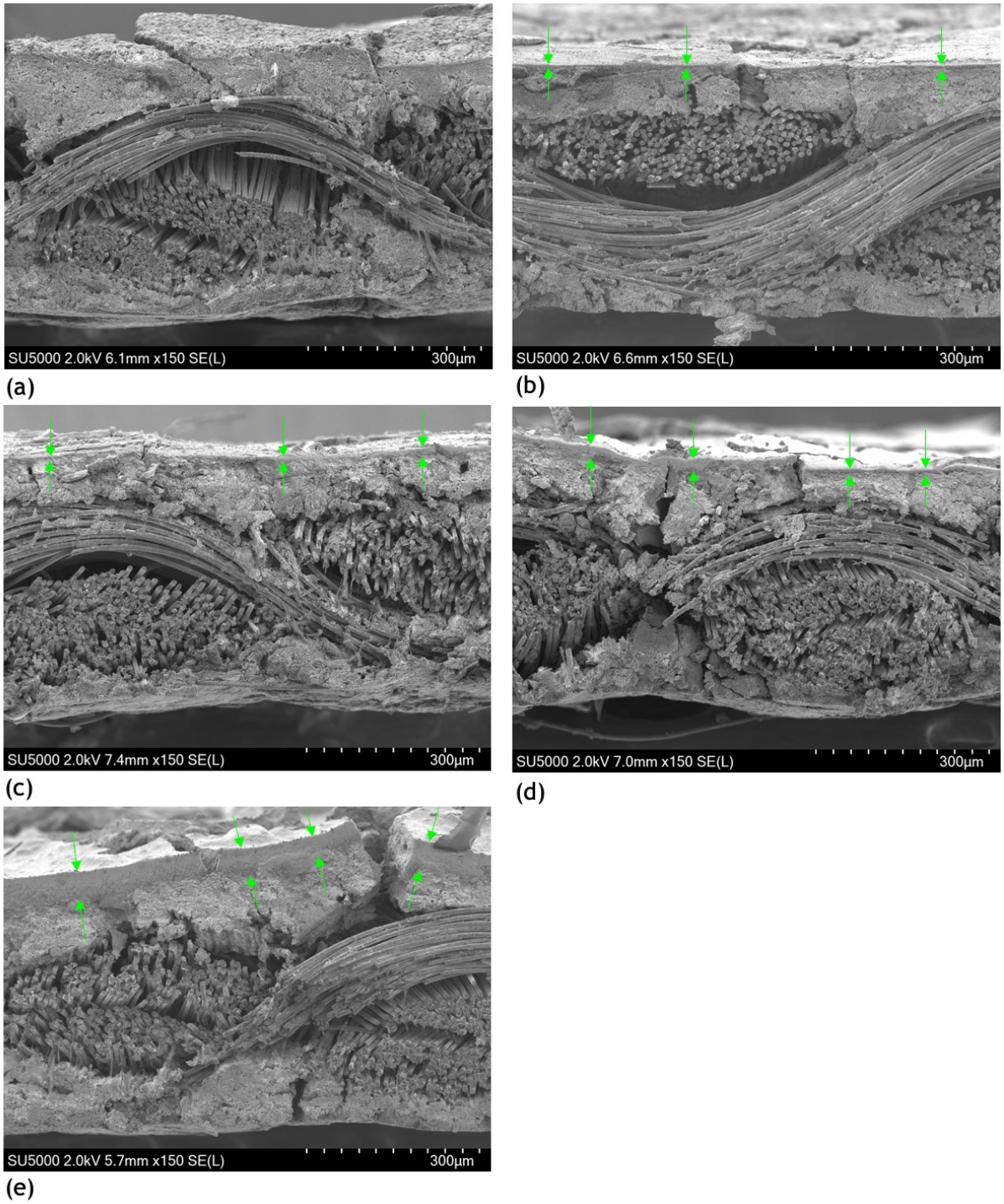

Figure 12. Cross-sectional SEM images of different electrocatalyst loadings at magnification of 150X: **(a)** control, **(b)** 0.5 mg/cm^2, **(c)** 1.5 mg/cm^2, **(d)** 3.0 mg/cm^2, **(e)** 5.0 mg/cm^2. The side coated with carbon ink is at the top of the photo with green arrows indicating the thickness of the electrocatalyst layer. The images were created using the S4800 SEM at the Clemson University Electron Microscopy Lab.

5.3 Effect of Electrocatalyst Ink Composition on H_2O_2 Production

The electrocatalyst loading study in the previous section along with its preceding research used the same composition of the electrocatalyst ink, with Nafion dispersion as liquid base for the carbon ink. The results in **Figure 13** display how the absence of Nafion in the electrocatalyst impacts the GDE's H_2O_2 production performance. The electrocatalyst loading trend observed in the previous results with Nafion is also evident for electrodes prepared without Nafion as the 1.5 mg/cm^2 achieved greater current efficiencies than 5.0 mg/cm^2. The H_2O_2 concentrations for the two loadings aligned very closely at each time point. The 5.0 mg/cm^2 loading achieved an average maximum H_2O_2 concentration of 876.10 mg/L, slightly outperforming the 1.5 mg/cm^2 loading, which produced an average maximum concentration 845.68 mg/L of H_2O_2 after 120 minutes. Regardless of the loading, the cathodes without Nafion in the electrocatalyst layer performed better than the cathodes with an electrocatalyst with Nafion. The Nafion dispersion used to create the carbon ink consists of a mixture of ethanol, propanol, and Nafion polymer. After the electrocatalyst is painted onto the MPL of the electrode and the surface is allowed to dry completely, the alcohol evaporates, leaving only Nafion and carbon on the electrode. Since the without Nafion results shown in **Figure 13** consist of a significantly smaller spread between loadings, the issue in lowered performance for higher loadings in the previous section must lie with the Nafion.

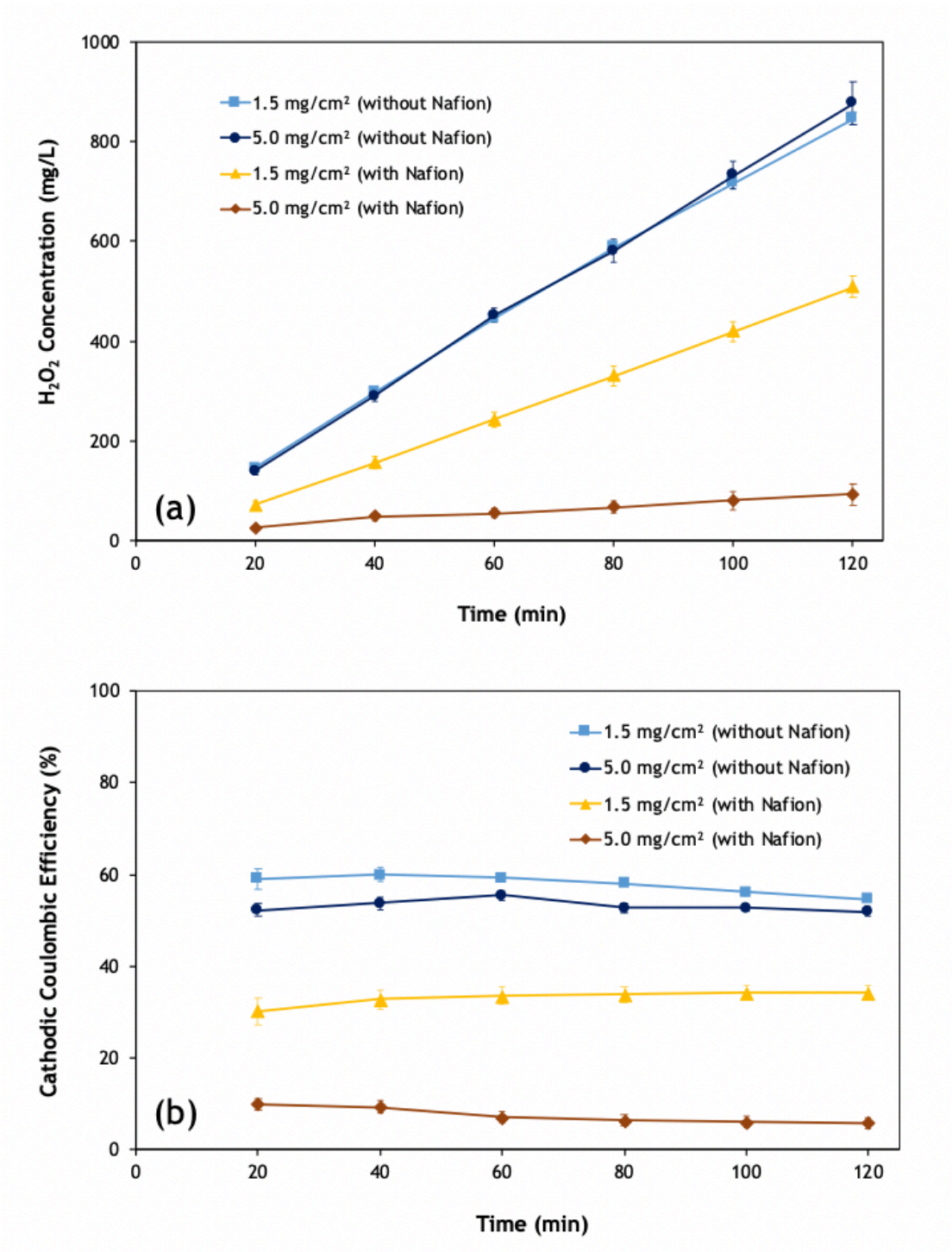

Figure 13. (a) H_2O_2 concentrations and **(b)** cathodic coulombic efficiencies for two electrocatalyst loadings with and without Nafion at a current density of **1 mA/cm^2**. Error bars represent standard error for quadruplicate trials.

Nafion is a random copolymer that consists of a hydrophobic PTFE backbone attached to a fully fluorinated pendant chain terminated with a strongly hydrophilic sulfonic acid group.[29] Applied in fuel cells as a cation exchange polymer, Nafion participates in proton hopping (through the Grotthuss mechanism), transporting H^+ ions from one SO_3^- group to another, as shown in the top illustration of **Figure 14**. It is expected that the pH at the surface of the cathode increases very quickly, resulting in peroxide being produced as its anion form, HO_2^-, rather than H_2O_2.When H_2O_2 exists in its uncharged form in the electrocatalyst layer, it is transported to the electrolyte through simple diffusion. However, when present in its charged species, HO_2^-, both the chemical and material (with Nafion) are then negatively charged and HO_2^- experiences friction with the SO_3^- groups with more resistance to movement. Overtime, the HO_2^- likely accumulates and gets degraded before it can diffuse out into the electrolyte. This transport mechanism supports the results in **Figure 13** in which electrocatalysts without Nafion clearly outperformed those with Nafion in regard to H_2O_2 concentrations produced and current efficiencies.

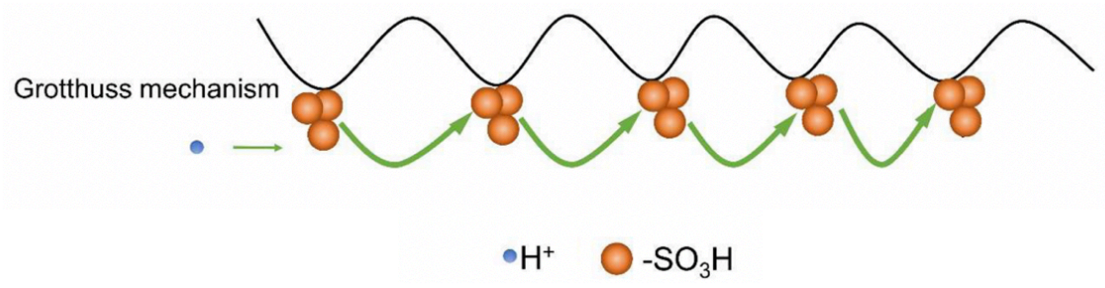

Figure 14. Schematic diagram of proton hopping mechanism with Nafion.[33]

5.3.1 SEM Images

In **Figure 15**, a side-by-side comparison at two magnification levels is shown for the 1.5 and 5.0 mg/cm^2 loadings applied with the electrocatalyst without Nafion. When Nafion is absent in the electrocatalyst ink, the interface between the electrocatalyst layer and MPL is not as defined as in the SEM images of the Nafion electrodes (**Figure 11** and **12**). The green overlays in **Figure 15** encompass the top MPL and electrocatalyst layer together. The thickness of the MPL is characteristic of the cathode cloth, so any increase in overall thickness of the cathode must be attributed to the electrocatalyst loading. Even without visually defining the start of the electrocatalyst layer, there is still a clear indication of an increase in electrocatalyst layer thickness when the loading is increased from 1.5 to 5.0 mg/cm^2. This observation further supports the previous discussion regarding Nafion restricting the movement of H_2O_2 through the electrocatalyst layer.

Prepared in a similar manner, the primary difference between the with and without Nafion electrodes is the presence of Nafion. When a higher electrocatalyst loading is applied, a greater mass of Nafion is present in the electrocatalyst layer. Therefore, in a cathode prepared with an electrocatalyst loading of 5.0 mg/cm^2, which contains about 10 times the amount of Nafion as in the 0.5 mg/cm^2 loading, the restriction of molecule movement by HO_2^- would be amplified. This conclusion aligns well with the H_2O_2 production results in **Figure 13** where the differences in H_2O_2 production and current efficiencies for the two electrocatalyst loadings is minimal for electrodes without Nafion when compared to with Nafion. Consequently, for a GDE with

an electrocatalyst layer deficient of Nafion, the effect of electrocatalyst loading is not as significant.

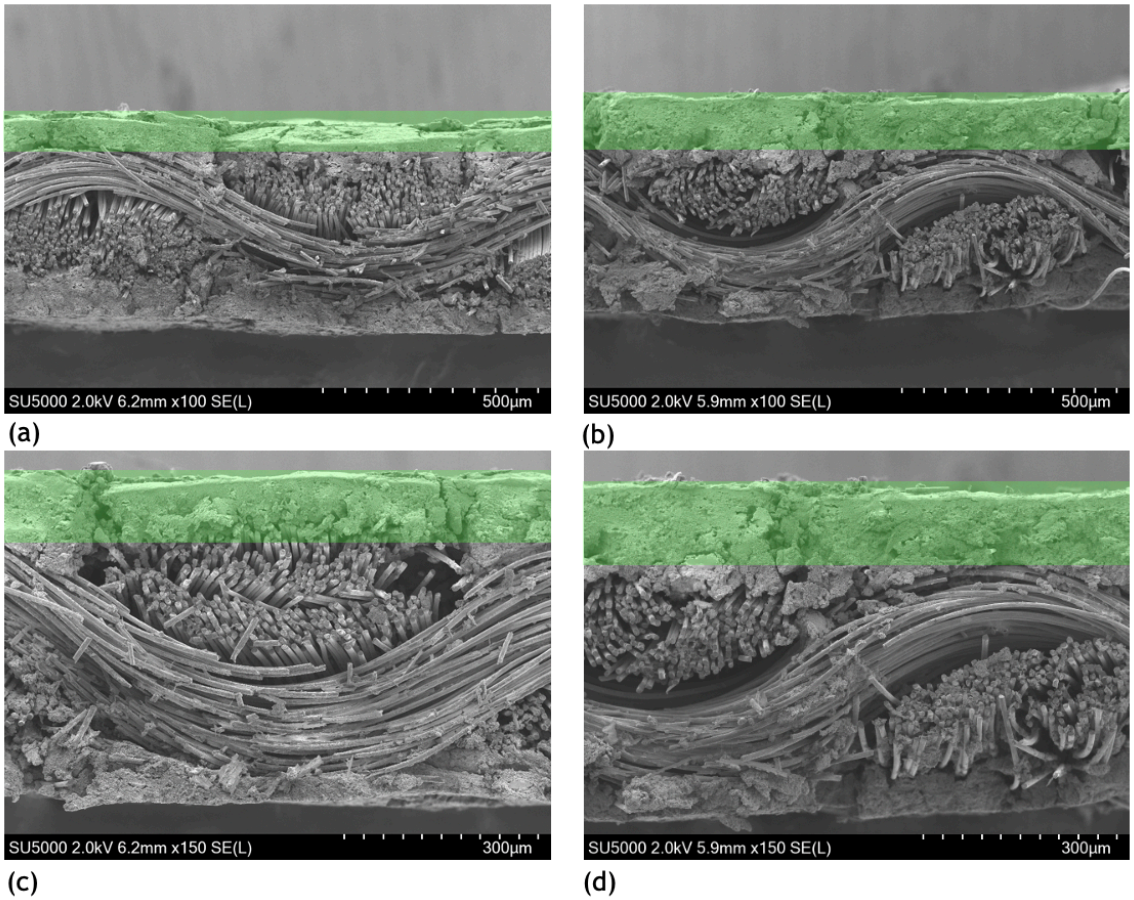

Figure 15. Cross-sectional SEM images of electrocatalyst loadings without Nafion at a magnification of 100X: **(a)** 1.5 mg/cm^2, **(b)** 5.0 mg/cm^2 and 150X: **(c)** 1.5 mg/cm^2, **(d)** 5.0 mg/cm^2. The side coated with carbon ink is at the top of the photo with a green overlay encompassing the thickness of the MPL and electrocatalyst layer. The images were created using the S4800 SEM at the Clemson University Electron Microscopy Lab.

5.4 Other Considerations

In addition to removing Nafion in the electrocatalyst ink composition, addition of a hydrophobic polymer, PTFE was evaluated to examine the effects of altering the hydrophobicity of the cathode surface. The results in **Figure 16** for the Nafion electrocatalysts show a clear difference between no PTFE and addition of PTFE to the

carbon ink. The average maximum H_2O_2 concentration achieved after 120 minutes was 508.79 mg/L for PTFE/CB=0 and 966.82 mg/L for PTFE/CB=1.6. A comparable observation is prominent for the efficiency as addition of the PTFE raised current efficiencies from 30-35% to 50-55%. The effect of PTFE on H_2O_2 production with an electrode prepared without Nafion is not as great as compared to with Nafion. Mass ratios of PTFE/CB=0 and 1.0 achieved almost identical current efficiencies in the range of 50-60%. However, an improvement in electrosynthesis with added PTFE can be observed with an increase in H_2O_2 concentration at 120 minutes from 845.68 mg/L to 1000.45 mg/L. It should be noted that only two trials were performed for PTFE/CB=1.0 and three trials for PTFE/CB=1.6.

It is known that efficient O_2 mass transfer and active sites for the ORR are crucial for efficient H_2O_2 production. When PTFE is introduced to the cathode surface, the hydrophobicity of the electrocatalyst layer is enhanced, decreasing the active sites for the ORR and improving the mass transfer of oxygen. PTFE is able to combat this challenge through the formation of a superhydrophobic interface, favoring the production of higher H_2O_2 concentrations and current efficiencies revealed in these results.[20]

The results in **Figure 16** demonstrate the benefits of adding PTFE to the electrocatalyst composition when Nafion is present in the carbon ink. Although adding PTFE to the electrocatalyst composition without Nafion showed improvement, more research would need be done to confirm that higher mass ratios of PTFE/CB would follow this trend. At this point, it can be concluded that addition of PTFE to a Nafion ink is justified and more mass ratios should be tested to determine an optimum condition.

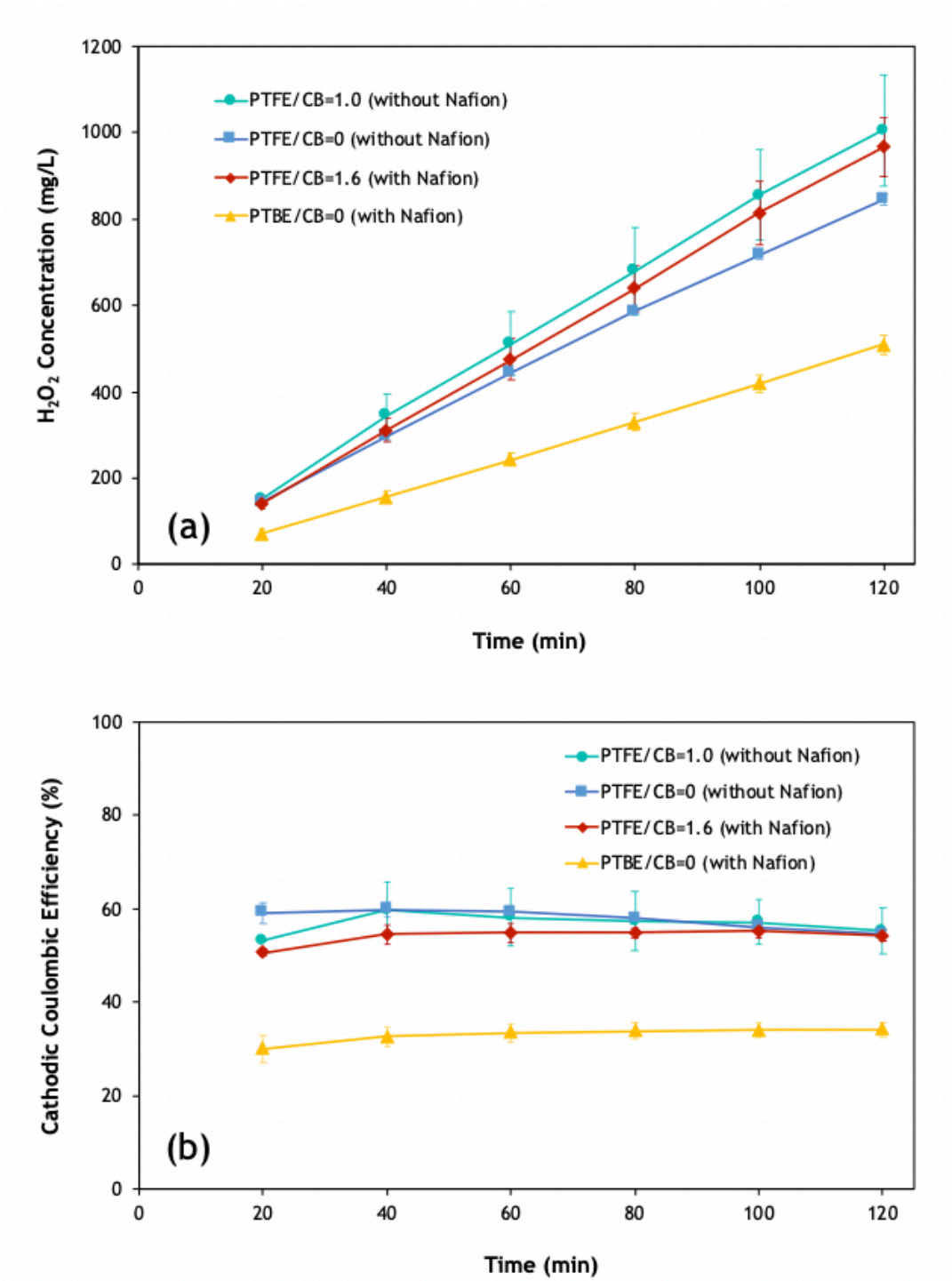

Figure 16. **(a)** H_2O_2 concentrations and **(b)** cathodic coulombic efficiencies for two PTFE/CB mass ratios with and without Nafion at a current density of **1 mA/cm^2** and electrocatalyst loading of **1.5 mg/cm^2**. Error bars represent standard error for quadruplicate trials.

6.0 CONCLUSION

6.1 Assessment of Research Objectives

6.1.1 ***Determine the effect of electrocatalyst loading on H_2O_2 production.*** An increase in electrocatalyst loading comprised of Vulcan carbon electrocatalyst ink with Nafion produced lower H_2O_2 production efficiencies and lower concentrations of H_2O_2 at a current density of 1.0 mA/cm^2. The highest applied current density of 9.0 mA/cm^2 produced the highest concentrations of H_2O_2 for all electrocatalyst loadings. The performance of the lowest electrocatalyst loading of 0.5 mg/cm^2 remained consistent across the range of applied current densities as it produced comparable cathodic coulombic efficiencies. At the current densities of 5.0 and 9.0 mA/cm^2, higher electrocatalyst loadings consistently improved performance as they increased in efficiencies that closely overlapped with those of the lower electrocatalyst loadings. At lower current densities, the differences in cathodic overpotential amongst the electrocatalyst loadings were minimal. Once the current density increased to 5.0 mA/cm^2, there were significant increases in the overpotential for all electrocatalyst loadings, with higher loadings requiring less external energy input. The energy input analysis revealed an advantage of choosing a higher loading at higher current densities to save on energy input costs, while still producing adequate H_2O_2 concentrations.

6.1.2 ***Examine the relationship between electrocatalyst loading and cathode structure.*** SEM images showed that the applied electrocatalyst formed a distinct electrocatalyst layer on the top of the gas diffusion layer in the cathode. Increased

loadings correlated to greater thicknesses of the electrocatalyst layers, with electrocatalyst loadings of 3.0 and 5.0 mg/cm^2 characterized by the most distinct layers. A greater thickness of electrocatalyst layer on top of the gas diffusion layer increases the path length required for H_2O_2 to diffuse into the electrolyte solution. For higher electrocatalyst loadings, this increases the difficulty and time for H_2O_2 to reach the electrolyte solution as well as the probability that it be degraded at the cathode surface.

6.1.3 *Determine the effect of electrocatalyst ink composition on H_2O_2 production.*

When Nafion was absent in the Vulcan carbon electrocatalyst ink, H_2O_2 concentrations and current efficiencies increased significantly. The two loadings tested for the without Nafion ink, 1.5 and 5.0 mg/cm^2, outperformed their counterparts prepared with Nafion ink. The higher loading of 1.5 mg/cm^2 did achieve higher current efficiencies than the 5.0 mg/cm^2 as observed in the with Nafion results. However, it was also observed that the loadings without Nafion achieved more similar H_2O_2 concentrations and efficiencies, with less of a range of values. A hydrophobic copolymer, Nafion contains strongly hydrophilic sulfonic acid groups, which are negatively charged. When in its anion form, HO_2^- has restricted movement through the electrocatalyst layer with the interaction of the negatively charged sulfonic acid groups. As a result, HO_2^- has more time and a greater potential to be degraded before reaching the electrolyte as compared to the electrocatalyst layer comprised of only carbon.

6.1.4 ***Other Considerations: Cathode Hydrophobicity.*** Preliminary results on altering the hydrophobicity of the cathode surface with the addition of PTFE suggest benefits of an increased hydrophobic surface. The with and without Nafion inks with PTFE each saw an improvement in H_2O_2 production and current efficiencies, where the with Nafion electrocatalyst had the greater improvement. For an electrocatalyst layer containing Nafion, the addition of PTFE is more justified for its significant improvement on the mass transfer and diffusion of H_2O_2 to the electrolyte. As only one PTFE/CB mass ratio was tested for each ink, smaller and greater mass ratios should be studied further to find an optimum design condition.

7.0 FUTURE WORK

This research aimed to improve the efficiency of the electrosynthesis of H_2O_2 on carbon black gas diffusion electrodes. The results on the modification of the electrocatalyst ink composition indicated a cation exchange polymer, such as Nafion, inhibits the mass transport of H_2O_2 through the electrocatalyst layer. A greater variation in loadings for electrocatalyst inks prepared without Nafion should be examined for a complete comparison against the electrocatalyst inks with Nafion. In addition to SEM imaging, additional characterization methods like X-ray CT scanning are recommended to further visualize the diffusion pathway and provide porosity measurements of the electrode infrastructure. Raman spectroscopy should also be utilized to further evaluate the electrocatalyst layer thickness and the impact the electrocatalyst ink composition has on the structure of the cathode infrastructure and gas diffusion layer.

Electrosynthesis of H_2O_2 using MPPCs provides a potential solution as a low-cost, low-energy technology. With the GDL driving the amount of H_2O_2 produced at the cathode, the modifications on the GDL performed in this study found ways to improve the efficiency of H_2O_2 production using a GDE. The electrosynthesis of H_2O_2 is advantageous for use in AOPs and EAOPs. Electrochemical treatment methods have become increasingly interesting as they are capable of treating wastewater with high toxicity and low biodegradability.[3] The improvements completed for the GDE performance at the cathode in this study should be implemented in an EAOP, such as Electro-Fenton oxidation, for in-situ electrogeneration of H_2O_2 at the cathode. Such improvements in H_2O_2 production would support formation of more hydroxyl radicals,

which can act as oxidants in removing recalcitrant organic matter in wastewater and landfill leachate, with the potential of improving wastewater treatment plant design.

APPENDICES

Appendix A – Pictures of electrochemical cell reactor and materials

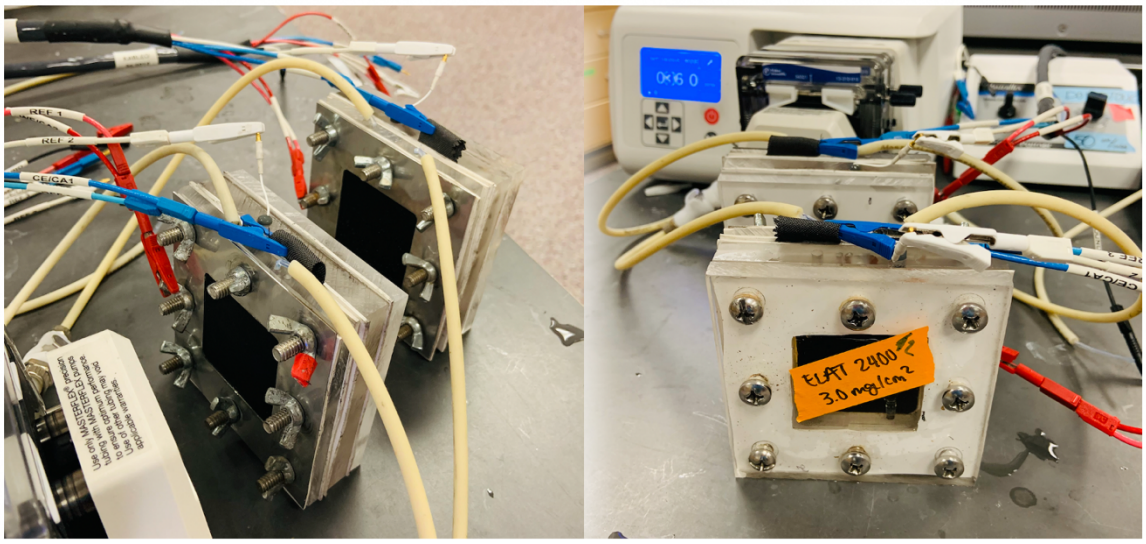

Figure A-1. Configuration for H_2O_2 production experiments with electrodes connected to potentiostat and a recirculation line through the cathode chamber.

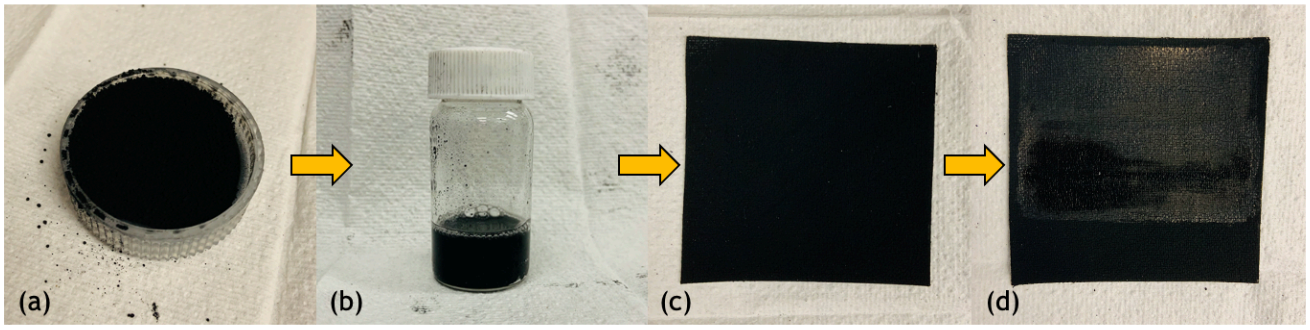

Figure A-2. Electrocatalyst ink and cathode preparation: **(a)** Vulcan XC 72 carbon powder, **(b)** carbon based electrocatalyst ink, **(c)** ELAT2400 bare cloth, **(d)** ELAT2400 painted with electrocatalyst.

Figure A-3. Spectrophotometric measurement of H_2O_2 standards using titanium oxysulfate method – concentration increases left to right.

Appendix B – Vulcan XC 72 Properties

Table B-1. Physical and chemical properties of Vulcan XC 72 carbon powder.[a]

Property	Value/Description
Appearance	Black Powder or Pellets
Odor	None
pH	4 - 11 [50 g/l water, 68°F (20°C)] (non-oxidized carbon black) 2 - 4 (oxidized carbon black)
Water Solubility	Insoluble
Average Particle Size	50 nm
Density	1.7 - 1.9 g/cm^3 @ 20°C
Bulk Density	200-680 kg/cm^3 (Pellets) 20-380 kg/m^3 (Fluffy)
% Volatile (by weight)	< 2.5% (950°C) (non-oxidized carbon black) 2 - 8% (oxidized carbon black)
Explosion Limits in Air - Lower	50 g/cm^3 (dust)
Autoignition Temperature	>140°C (transport)

[a]Properties attained from: *Vulcan XC72;* MSDS; Fuel Cell Store: College Station, TX, December 04, 2012.

Appendix C – pH data

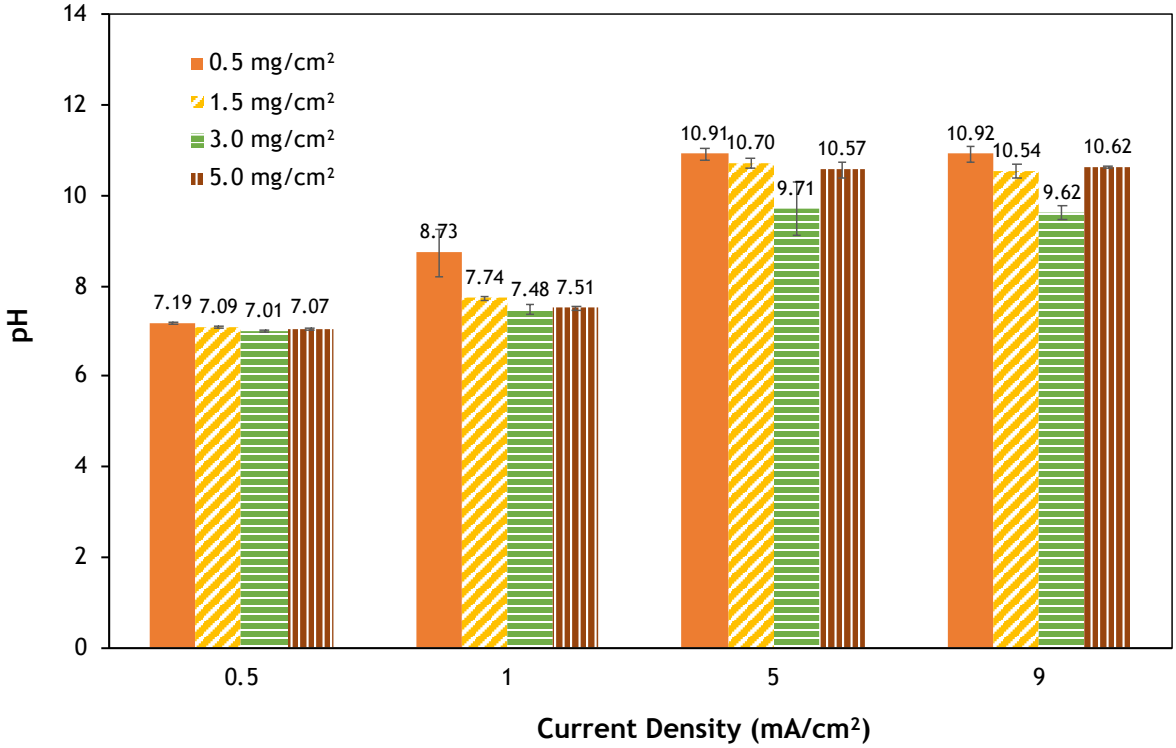

Figure C-1. Average final cathode pH from electrocatalyst loading experiments. Error bars represent standard error for quadruplicate trials.

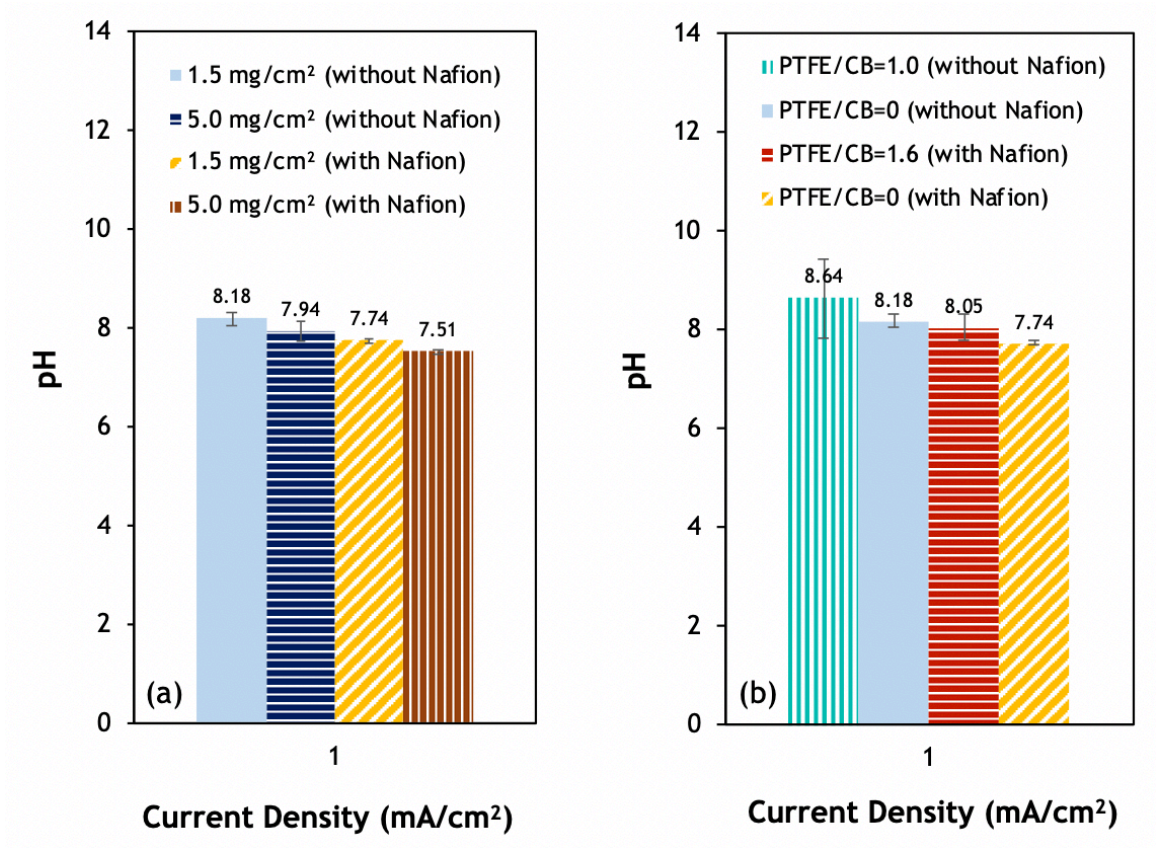

Figure C-2. Average final cathode pH from electrocatalyst ink composition experiments for **(a)** two electrocatalyst loadings with two different inks and **(b)** two PTFE/CB mass ratios with two different inks and an electrocatalyst loading of **1.5 mg/cm²**. Error bars represent standard error for quadruplicate trials.

Appendix D – Additional SEM images for electrocatalyst loading experiments

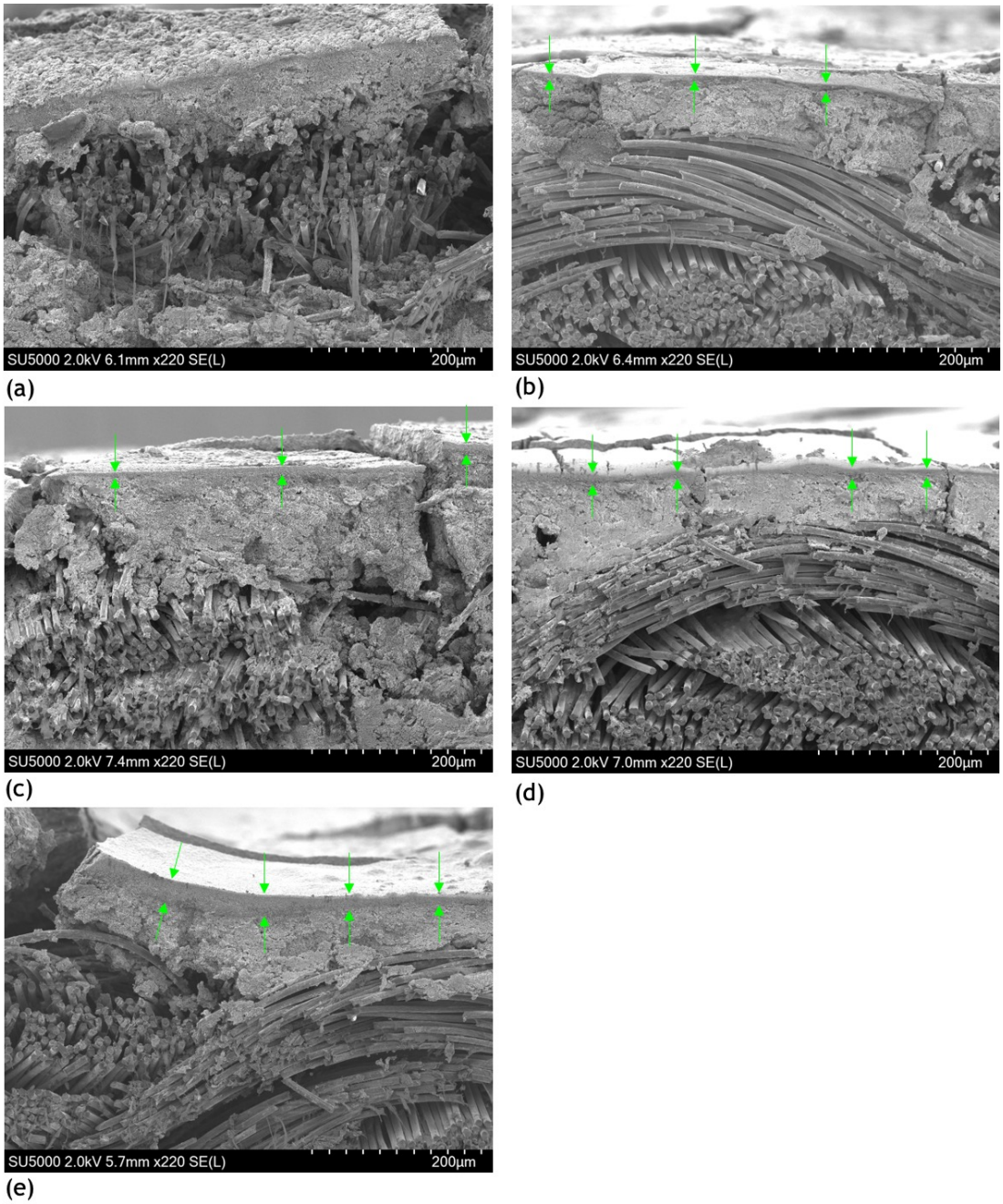

Figure D-1. Cross-sectional SEM images of different electrocatalyst loadings at magnification of 220X: **(a)** control, **(b)** 0.5 mg/cm^2, **(c)** 1.5 mg/cm^2, **(d)** 3.0 mg/cm^2, **(e)** 5.0 mg/cm^2. The side coated with carbon ink is at the top of the photo with green arrows indicating the thickness of the electrocatalyst layer. The images were created using the S4800 SEM at the Clemson University Electron Microscopy Lab.

REFERENCES

(1) W. Yao, J.Fu, H. Yang, G. Yu, and Y. Wang, "The beneficial effect of cathodic hydrogen peroxide generation on mitigating chlorinated by-product formation during water treatment by an electro-peroxone process," *Water Research*, vol. 157, pp. 209-217.

(2) A. Y. Bagastyo, D. J. Bastone, I. Kristiana, W. Gernjak, C. Joll, and J. Radjenovic, "Electrochemical oxidation of reverse osmosis concentrate on boron-doped diamond anodes at circumneutral and acidic pH," *Water Research*, vol. 46, pp. 6104-6112, 2012.

(3) M. N. Young, N. Chowdhury, E. Garver, P. J. Evans, S. C. Popat, B. E. Rittmann, and C. I. Torres, "Understanding the impact of operational conditions on performance of microbial peroxide producing cells," *Journal of Power Sources*, vol. 356, pp. 448–458, 2017.

(4) J. Chen, L. Zhao, N. Li, and H. Liu, "A microbial fuel cell with the three-dimensional electrode applied an external voltage for synthesis of hydrogen peroxide from organic matter," *Journal of Power Sources*, vol. 287, pp. 291-296, 2015.

(5) J. Chen, N. Li, and L. Zhao, "Three-dimensional electrode microbial fuel cell for hydrogen peroxide synthesis coupled to wastewater treatment," *Journal of Power Sources*, vol. 254, pp. 316-322, 2014.

(6) Q. Chen, "Development of an anthraquinone process for the production of hydrogen peroxide in a trickle bed reactor – From bench scale to industrial scale," *Chemical Engineering and Processing*, vol. 47, pp. 787-792, 2008.

(7) J. M. Campos-Martin, G. Blanco-Brieva, and J. L. G. Fierro, "Hydrogen Peroxide Synthesis: An Outlook beyond the Anthraquinone Process," *Angewandte Chemie*, vol. 45, pp. 6962-6984, 2006.

(8) C. Prat, M. Vicente, and S. Esplugas, "Treatment of bleaching waters in the paper industry by hydrogen peroxide and ultraviolent radiation," *Water Research*, vol. 22, pp. 663-668, 1988.

(9) M. Muruganandham and M. Swaminathan, "Photochemical oxidation of reactive azo dye with UV-H_2O_2 process," *Dyes and Pigments*, vol. 62, pp. 269-275, 2004.

(10) C. Jung, Y. Deng, R. Zhao, and K. Torrens, "Chemical oxidation for mitigation of UV-quenching substances (UVQS) from municipal landfill leachate: Fenton process versus ozonation," *Water Research*, vol. 108, pp. 260-270, 2017.

(11) E. Atmaca, "Treatment of landfill leachate by using electro-Fenton method," *Journal of Hazardous Materials*, vol. 163, pp. 109-114, 2009.

(12) M. Panizza, and G. Cerisola, "Electro-Fenton degradation of synthetic dyes," *Water Research*, vol. 43, pp. 339-344, 2009.

(13) E. Brillas, I. Sires, and M. A. Oturan, "Electro-Fenton Process and Related Electrochemical Technologies Based on Fenton's Reaction Chemistry," *Chem. Rev.*, vol. 109, pp. 6570-6631, 2009.

(14) R. A. Rozendal, E. Leone, J. Keller, and K. Rabaey, "Efficient hydrogen peroxide generation from organic matter in a bioelectrochemical system," *Electrochemistry Communications*, vol. 11, pp. 1752-1755, 2009.

(15) N. Li, Y. Liu, J. An, C. Feng, and X. Wang, "Bifunctional quaternary ammonium compounds to inhibit biofilm growth and enhance performance for activated carbon air-cathode in microbial fuel cells," *Journal of Power Sources*, vol. 272, pp. 895-899, 2014.

(16) Rabaey, K.; Verstraete, W. Microbial Fuel Cells: Novel Biotechnology for Energy Generation. *Trends Biotechno*l. 2005, 23 (6), 291–298.

(17) K. Watanabe, "Recent Developments in Microbial Fuel Cell Technologies for Sustainable Bioenergy," *Journal of Bioscience and Bioengineering*, vol. 106, pp. 528–536, 2008.

(18) Z. Yu, M. Zhou, G. Ren, and L. Ma, "A novel dual gas diffusion electrodes system for effieicient hydrogen peroxide generation used in electro-Fenton," *Chemical Engineering Journal*, vol. 263, pp. 92-100, 2015.

(19) R. M. Reis, A. A. G. F. Beati, R. S. Rocha, M. H. M. T. Assumpcao, M. C. Santos, R. Bertazzoli, and M. R. V. Lanza, "Use of Gas Diffusion Electrode for the In Sity Generation of Hydrogen Peroxide in an Electrochemical Flow-By Reactor," *Industrial & Engineering Chemistry Research*, vol. 51, pp. 649-654, 2012.

(20) Q. Zhang, M. Zhou, G. Ren, Y. Li, and X. Du, "Highly efficient electrosynthesis of hydrogen peroxide on a superhydrophobic three-phase interface by natural air diffusion," *Nature Communications*, vol. 11, 2020.

(21) Y. Sheng, S. Song, X. Wang, L. Song, C. Wang, H. Sun, and X. Niu, "Electrogeneration of hydrogen peroxide on a novel highly effective acetylene black-PTFE cathode with PTFE film," *Electrochimica Acta*, vol. 56, pp. 8651-8656, 2011.

(22) W. R. P. Barros, R. M. Reis, R. S. Rocha, and M. R. V. Lanza, "Electrogeneration of hydrogen peroxide in acidic medium using gas diffusion electrodes modified with cobalt (II) phthalocyanine," *Electrochimica Acta*, vol. 104, pp. 12-18, 2013.

(23) P. Ding, L. Cui, D. Li, and W. Jing, "Innovative Dual-Compartment Flow Reactor Coupled with a Gas Diffusion Electrode for in Situ Generation of H_2O_2," *Industrial & Engineering Chemistry Research*, vol. 58, pp. 6925-6932, 2019.

(24) E. Brillas, R. M. Bastida, E. Llosa, and J. Casado, "Electrochemical destruction of aniline and 4-chloroaniline for wastewater treatment using a carbon-PTFE O_2-fed cathode" *Journal of Electrochemical Society*. vol. 142, pp. 1733–1741, 1995.

(25) C. A. Martinez-Huitle, and E. Brillas, "Decontamination of wastewaters containing synthetic organic dyes by electrochemical methods: a general review," *App. Catal. B*, vol. 87, pp. 105–145, 2009.

(26) E. L. Murawski, "Optimizing Cathode Catalyst Loading in Microbial Peroxide-Producing Cells for Greywater Disinfection," Clemson University, 2018.

(27) S. C. Lindsay, "Effect of Electrolyte pH on the Electrosynthesis of Hydrogen Peroxide on Carbon Black-Based Gas Diffusion Electrodes," Clemson University, 2020.

(28) Bonakdarpour, A.; Lefevre, M.; Yang, R.; Jaouen, F.; Dahn, T.; Dodelet, J.- P.; Dahn, J. R. Impact of Loading in RRDE Experiments on Fe–N–C Catalysts: Two- or Four-Electron Oxygen Reduction? *Electrochem. Solid- State Lett*. 2008, 11 (6), B105.

(29) R. Devanathan, A. Venkatnathan, R. Rousseau, M. Dupuis, T. Frigato, W. Gu, and V. Helms, "Atomistic Simulation of Water Percolation and Proton Hopping in Nafion Fuel Cell Membrane," J. *Phys. Chem. B*, vol. 114, pp. 13681-13690, 2010.

(30) M. N. Young, M. J. Links, S. C. Popat, B. E. Rittmann, and C. I. Torres, "Tailoring Microbial Electrochemical Cells for Production of Hydrogen Peroxide at High Concentrations and Efficiencies," *ChemSusChem*, vol. 9, pp. 1-9, 2016.

(31) Arends, J. B. A.; Denhouwe, S. Van; Verstraete, W.; Boon, N.; Rabaey, K. Bioresource Technology Enhanced Disinfection of Wastewater by Combining Wetland Treatment with Bioelectrochemical H2O2 Production. *Bioresour. Technol*. 2014, 155, 352–358.

(32) Biddinger, E. J.; Deak, D. von; Singh, D.; Marsh, H.; Tan, B.; Knapke, D. S.; Ozkan, U. S. Examination of Catalyst Loading Effects on the Selectivity of CNx and Pt/VC ORR Catalysts Using RRDE. *J. Electrochem*. Soc. 2011, 158 (4), B402.

(33) S. Zhai, W. Dai, J. Lin, S. He, B. Zhang, and L. Chen, "Enhanced Proton Conductivity in Sulfonated Poly(ether ether ketone) Membranes by Incorporating Sodium Dodecyl Benzene Sulfonate," *Polymers*, vol. 11, 2019.